Neonatal hypofunction of NMDA receptors alters perforant path synaptic plasticity, filtering and impairs dentate gyrus-mediated spatial discrimination

Luis Alfredo Márquez[1], Carolina Lopez-Rubalcava[2], and Emilio Galvan[1]

[1]CINVESTAV Departamento de Farmacobiología Sede Sur
[2]CINVESTAV Departamento de Farmacobiología

September 5, 2023

Abstract

Background and Purpose: Transient hypofunction of NMDARs represents a convergence point for the onset and further development of psychiatric disorders, including schizophrenia. Although the cumulative evidence indicates dysregulation of the hippocampal formation in schizophrenia, the integrity of the synaptic transmission and plasticity conveyed by the somatosensorial inputs to the dentate gyrus, the perforant path synapses, have barely been explored in this pathological condition. Experimental Approach: We identified a series of synaptic alterations of the lateral and medial perforant paths, in animals neonatally treated with the NMDAR antagonist MK-801. The dysregulation here reported suggests decreased cognitive performance, for which the dentate gyrus is critical. Key Results: We identified alterations in the synaptic properties of the lateral and medial perforant paths to the dentate gyrus synapses in MK-801-treated animals. Altered glutamate release and decreased synaptic strength precede an impairment in the induction and expression of LTP and cannabinoid 1 receptor (CB1R)-mediated LTD. Remarkably, by inhibiting the degradation of 2-arachidonoylglycerol, the endogenous ligand of the CB1R, we restored the LTD in animals treated with MK-801. Additionally, we show for the first time that spatial discrimination, a cognitive task that requires dentate gyrus integrity, is impaired in animals exposed to transient hypofunction of NMDARs. Conclusion and Implications: Descriptive and mechanistic evidence showing the dysregulation of glutamatergic transmission and synaptic plasticity from the entorhinal cortex to the dentate gyrus is presented. These findings may explain the cellular dysregulations underlying the altered cognitive processing in the dentate gyrus associated with schizophrenia.

Neonatal hypofunction of NMDA receptors alters perforant path synaptic plasticity, filtering and impairs dentate gyrus-mediated spatial discrimination

Luis A. Márquez[1], Carolina López Rubalcava[1] and Emilio J. Galván[1,2*]

[1]Departamento de Farmacobiología, CINVESTAV Unidad Sur, Ciudad de México, México.

[2]Centro de Investigaciones sobre el Envejecimiento, CIE-Cinvestav, Ciudad de México, México.

Running title: *Transient hypofunction of NMDARs alters dentate gyrus functionality*

***Address correspondence to:**

Dr. Emilio J. Galván

[1]Departmento de Farmacobiología

Centro de Investigación y Estudios Avanzados del Instituto Politécnico Nacional

Calzada de los Tenorios No. 235, Col. Granjas Coapa C.P. 14330, México

Phone: +52(55)5483-2852

Email: *ejgalvan@cinvestav.mx*

CRediT authorship contribution statement: Márquez : Conceptualization, Methodology, Formal analysis, Investigation, Writing – original draft preparation; **Lopez-Rubalcava** : Resources and Visualization; **Galván** : Conceptualization, Resources, Visualization, Writing – review and editing.

Bullet point summary:

What is already known

Hypofunction of NMDA receptors is a convergence mechanism for developing psychiatric diseases involving hippocampal dysregulation.

Preclinical and clinical evidence suggests physiological and behavioral dysregulation of the dentate gyrus, the hippocampus's sensorial gate.

What this study adds

Neonatal administration of MK-801 modifies LTP, LTD in the dentate gyrus and reduces spatial discrimination.

Enhancing 2-AG – CB1R signaling via MAGL inhibition restores long-term depression in MK-801-treated hippocampal slices.

Clinical significance

Mnemonic discrimination performance could help identify individuals at high risk for developing schizophrenia.

Cannabinoid system modulation may improve dentate gyrus-dependent synaptic and behavioral capabilities in schizophrenic individuals.

Keywords: MK-801, perforant path, dentate gyrus, cannabinoid receptor 1, MAGL, spatial discrimination, schizophrenia

Abstract

Background and Purpose : Transient hypofunction of NMDARs represents a convergence point for the onset and further development of psychiatric disorders, including schizophrenia. Although the cumulative evidence indicates dysregulation of the hippocampal formation in schizophrenia, the integrity of the synaptic transmission and plasticity conveyed by the somatosensorial inputs to the dentate gyrus, the perforant path synapses, have barely been explored in this pathological condition.

Experimental Approach : We identified a series of synaptic alterations of the lateral and medial perforant paths, in animals neonatally treated with the NMDAR antagonist MK-801. The dysregulation here reported suggests decreased cognitive performance, for which the dentate gyrus is critical.

Key Results : We identified alterations in the synaptic properties of the lateral and medial perforant paths to the dentate gyrus synapses in MK-801-treated animals. Altered glutamate release and decreased synaptic strength precede an impairment in the induction and expression of LTP and cannabinoid 1 receptor (CB_1R)-mediated LTD. Remarkably, by inhibiting the degradation of 2-arachidonoylglycerol, the endogenous ligand of the CB_1R, we restored the LTD in animals treated with MK-801. Additionally, we show for the first time that spatial discrimination, a cognitive task that requires dentate gyrus integrity, is impaired in animals exposed to transient hypofunction of NMDARs.

Conclusion and Implications : Descriptive and mechanistic evidence showing the dysregulation of glutamatergic transmission and synaptic plasticity from the entorhinal cortex to the dentate gyrus is presented.

These findings may explain the cellular dysregulations underlying the altered cognitive processing in the dentate gyrus associated with schizophrenia.

Introduction

A growing body of evidence indicates that hypofunction of N-methyl-D-aspartate receptors (NMDARs) represents a convergence point for the onset and further development of psychiatric disorders, including autism and schizophrenia (Snyder and Gao, 2013; Forsyth and Lewis, 2017; Nakazawa and Sapkota, 2020). The genetic/chemogenetic ablation or pharmacological blockade of NMDARs during critical periods of brain development has successfully reproduced the negative, cognitive, and psychotic symptoms associated with schizophrenia (Jeevakumar et al., 2015; Kjaerby et al., 2017; Seshadri et al., 2018; Nakao et al., 2019; Segev et al., 2020). Therefore, hypofunction of NMDARs by neonatal blockade with antagonists such as MK-801 leads to alterations in the release process of dopamine, glutamate, and GABA (Nakao et al., 2019; Segev et al., 2020; Márquez et al., 2023); alterations in the functional expression of ion channels and postsynaptic receptors in the hippocampus (Griego et al., 2022; Márquez et al., 2023); and behavioral deficits that resemble the negative and cognitive symptoms of schizophrenia (Kjaerby et al., 2017; Seshadri et al., 2018; Segev et al., 2020).

It is now accepted that the hippocampus, a brain region essential for cognitive processing, the formation of new memories (Eichenbaum, 2004; Nadel et al., 2012), and the development of social behaviors (Lopez-Rojas et al., 2022), is central in the pathophysiology of schizophrenia (Tamminga et al., 2010; Segev et al., 2020). In line with this tenet, the dentate gyrus (DG), the somatosensorial gate of the hippocampus, shows the greatest volumetric loss, neuroanatomic disorganization, and altered glutamatergic/GABAergic transmission in schizophrenic individuals and animal models (Li et al., 2015; Stan et al., 2015; Nakahara et al., 2019; Griego et al., 2022). The DG receives and processes somatosensorial and spatial information from the entorhinal cortex via the lateral perforant pathway (LPP) and the medial perforant pathway (MPP), respectively (Hunsaker et al., 2007; Fernández-Ruiz et al., 2021), and minimizes the overlapping of new memories with highly similar content via a theoretical mechanism known as pattern separation (Yassa and Stark, 2011).

Additionally, multiple works have shown the relevance of the cannabinoid 1 receptor (CB_1R) for the induction of long-term depression and potentiation in the PP – DG synapses (Wu et al., 2006; Wang et al., 2016, 2018b; Peñasco et al., 2019; Fontaine et al., 2020). Interestingly, dysregulation of NMDARs and CB_1R is present in animal models and schizophrenic individuals (Szűcs et al., 2016; Forsyth and Lewis, 2017; Osborne et al., 2019; Márquez et al., 2023). Despite the potential repercussions of the altered functionality of NMDARs and CB_1R within the LPP and MPP – DG synapses, little is known about the possibly altered functionality of the DG in schizophrenia.

This study identified neurophysiological alterations endured by LPP and MPP – DG synapses in response to the transient hypofunction of NMDARs during early postnatal development. The changes in the neurotransmitter release process, altered synaptic strength, and dysregulated synaptic filtering found in these synapses are accompanied by changes in the induction and expression of LTP and LTD and dysfunction of the presynaptic activity of the CB_1R. We also demonstrated that induction of LTD is restored by fostering the 2-Arachidonoylglycerol (2-AG) signaling, the endogenous ligand of the CB1R, via negative modulation of monoacylglycerol lipase (MAGL). Finally, we show for the first time that spatial discrimination, a cognitive task in which the DG takes part, deteriorates in response to neonatal hypofunction of NMDARs.**Methods**

Animals and neonatal treatment with MK-801

All our experimental procedures were carried out in rigorous accordance with the "NOM-062-ZOO-1999" local regulation for the use and care of laboratory animals and the protocols authorized by the internal ethics committee (CICUAL) of our institution (CINVESTAV; Protocol number 0090-14), which mandate the minimization of suffering and the number of experimental animals used. These regulations and protocols are consistent with the ARRIVE 2.0 guidelines, the recommendations made by the British Journal of Pharmacology (Lilley et al., 2020), and the National Institutes of Health (US) guidelines for animal care.

Pregnant Wistar rats were supplied by our vivarium and given continuous veterinary care. The rats were housed in the following control conditions: an inverted light-dark cycle (12 h; the light was turned off at 10:00 h), a room temperature of 23 ± 1° C, and free access to food and water. The pups' birth was designated as postnatal day 0 (P0), and animals were kept with their mothers until P21. The experimental procedures were performed in two cohorts of male animals ranging from 30 to 38 days old. Each experimental manipulation was carried out in at least three different litters. From P7 to P11, the animals received daily subcutaneous injections of either saline solution (SS, 0.9%) or MK-801 (0.2 mg/kg in a 2 mL/kg volume) (Griego et al., 2022; Márquez et al., 2023). The behavioral procedures were carried out between 10:00 and 16:00 h. The experimental animals were treated with SS or MK-801, following a single sequence of random assignments. The MK-801 was dissolved in isotonic SS. Animal suffering was minimized during and after the injections to reduce behavioral or neurophysiological alterations that might affect the experimental results. In addition, the assignment of animals to control and MK-801 groups was blind, to prevent any potential bias.

Acute slice preparation

Sodium pentobarbital (50 mg/kg in a 1 mL/kg volume) was used for deep anesthesia; animals were then decapitated under its effects. Once removed from the skulls, brains were placed into a frosty sucrose solution containing (in mM): 210 sucrose, 2.8 KCl, 2 $MgSO_4$, 1.25 Na_2HPO_4, 25 $NaHCO_3$, 1 $MgCl_2$, 1 $CaCl_2$, and 10 D-glucose. The sucrose solution was continuously bubbled with a carbogen mixture (95% O_2/5% CO_2). Tissue blocks of cerebral hemispheres containing the hippocampus and surrounding areas were sliced at 385 µm thickness in the transversal plane using a vibrating tissue slicer (Leica VT1000S; Nusschloc, Germany). Next, the fresh slices were stabilized at 34° C for 25 to 30 min in an artificial cerebrospinal fluid solution (ACSF; pH [?] 7.30–7.35) containing (in mM): 125 NaCl, 2.5 KCl, 1.25 Na_2HPO_4, 25 $NaHCO_3$, 4 $MgCl_2$, 1 $CaCl_2$, and 10 D-glucose. Next, the slices were kept at room temperature for at least 1 hour before any experimental procedure was performed. An individual slice was transferred to a submerged chamber (total volume: 400 µL). The slice was continuously perfused with modified ACSF at a rate of 2.2–2.5 mL/min, with the help of a peristaltic pump (Sci Q400, Watson-Marlow, Wilmington, MA, USA). The modified ACSF (with continuous carbogen bubbling) included the following components (in mM): 125 NaCl, 2.5 KCl, 1.25 Na_2HPO_4, 25 $NaHCO_3$, 1.5 $MgCl_2$, 2.5 $CaCl_2$, and 10 D-glucose. The recordings were performed at 32.5 ±1 °C.

Extracellular recordings

Extracellular recordings were used to determine the synaptic properties of the MPP – DG synapse or the LPP – DG synapse acquired from the supra-pyramidal blade of the DG (see schematic representation in Figure 1a). The MPP field excitatory postsynaptic potentials (MPP fEPSPs) or the LPP fEPSPs were evoked with a bipolar nichrome electrode placed in the middle one-third or outer one-third section of the DG's molecular layer, respectively. The evoked fEPSPs were recorded with a borosilicate pipette (1-2 MΩ of tip resistance, when filled with NaCl solution, 3M) and placed 200-300 µM from the stimulation electrode. The current pulses were delivered via a high-voltage isolation unit (A365D; World Precision Instruments, Sarasota, FL, USA), commanded with a Master-8 pulse generator (AMPI, Jerusalem, Israel). Responses were amplified with a Dagan BVC-700A amplifier (Minneapolis, MN, USA) connected with a 100x gain headstage (Dagan, model 8024) and high-pass filtered at 0.3 Hz. Electrical noise suppression was accomplished with a Humbug noise eliminator (Quest Scientific Instruments; North Vancouver, BC, Canada). The evoked fEPSPs were displayed on a computer-based oscilloscope and digitalized for storage and offline analysis with LabVIEW 7.1 software (National Instruments, Austin, TX, USA). The A/D converter device used was the BNC-2110 (National Instrument, Austin, TX).

Determination of basal synaptic strength and paired-pulse ratio

A series of input-output (I-O) curves of current vs. synaptic responses was constructed by delivering increasing current pulses at 0.067 Hz from 0 to 800 µA (100 µA steeps, 100 µs duration) and measuring the evoked fEPSP amplitude (in mV). From the I-O curves, we also analyzed the Fiber volley (FV) amplitude in response to current injection to determine presynaptic excitability. The basal synaptic strength was determined by

analyses of the FV amplitude vs. fEPSP slope fitted with a Boltzmann function, and the differences between control and MK-801-treated slices were compared using the resulting slope of the Boltzmann equation. For short-term plasticity determined by paired-pulse ratio (PPR) analysis, a paired stimulation at 0.067 Hz (15-20% of evoked maximal fEPSP amplitude) was obtained, with inter-stimulus intervals (ISI) of 40, 60, 100, 200, and 500 ms. The PPR was calculated as the ratio between the amplitude of the second response (S2) and the amplitude of the first response (S1) (PPR = S2/S1). The input-specific origins of synaptic responses from the MPP and the LPP were corroborated by the preferential pharmacological sensitivity to DCG-IV (5 μM) and L-AP4 (20 μM), respectively (Macek et al., 1996).

Long-term plasticity: depression and synaptic potentiation

Because homosynaptic long-term depression (LTD) has scarcely been examined in the two anatomical divisions of the perforant path to the DG, different patterns of low-frequency stimulation (LFS) were used to examine the LPP's and MPP's susceptibility to express a stable LTD. A baseline response of fEPSP slope (50-70% of maximal fEPSP amplitude) was acquired with paired stimulation (60 ms ISI, 100 μs duration of current pulse) at 0.067 Hz for 20 min. Then, 900 unitary current pulses at 1-3 Hz were delivered at the LPP or the MPP, and the synaptic responses were recorded for 90 min. This was followed by pharmacological identification with L-AP4 or DCG-IV (Macek et al., 1996). In the case of MPP – DG synapse, LFS at 3 Hz was examined in the presence of the inverse agonist AM 251 (5 μM), to determine the dependence of cannabinoid receptor 1 (CB1) during the induction of LTD. For long-term potentiation (LTP) experiments, the baseline conditions and pharmacological identification were identical to those in the LTD experiments, except that the baseline response of the fEPSP slope was configured at 25-35% of its maximal amplitude. Then, a theta-burst stimulation (TBS) protocol was delivered to the LPP or the MPP, and synaptic responses were recorded for 90 minutes. The TBS protocol (based on Larson and Munkácsy, 2015) consisted of 3 episodes repeated at 10 s, each with 10 bursts at 5 Hz and 5 current pulses at 100 Hz (see Supplementary Figure 2). The decay of post-tetanic potentiation (PTP) induced by TBS was expressed as ? value, obtained from adjusting the best fit of individual fEPSP slope values with a nonlinear regression function of one phase decay. Heatmaps were constructed to depict the magnitude of LTP, and cumulative probability charts were constructed using post-TBS fEPSP slope values from minute 11 to 90.

Pharmacological modulation of 2-AG signaling pathway

In a subset of experiments focused on the MPP – DG synapse from control and MK-801-treated slices, WIN 55,212-2, a CB_1R agonist (WIN, 5 μM), was bath perfused for 15 minutes to examine the presynaptic induction of LTD mediated by CB_1 receptor activation, as previously reported (Fontaine et al., 2020). Additionally, physostigmine (10 μM), an acetylcholinesterase inhibitor, was perfused for 15 min to evaluate endogenous 2-AG production in the MPP – DG synapse, as previously demonstrated in acute hippocampal slices (Wang et al., 2018b, 2018a). Finally, in another subset of experiments, JZL 184 (1 μM), an irreversible inhibitor of monoacylglycerol lipase (MAGL) that increases the 2-AG levels (Wang et al., 2016) was perfused for 15 min on MK-801-treated slices to examine the effects of MAGL inhibition during the delivery of LFS at 3 Hz.

Determination of frequency-dependent filtering in the LPP – DG synapse

Synaptic frequency-dependent filtering was examined in the presence of DCG-IV (5 μM), and a baseline response of fEPSP slope configured at 50% of its maximal amplitude was acquired for 10-12 min. Then, a train of 10 current pulses (100 μs of duration) at 5, 20, and 50 Hz was delivered to the LPP, with an interval of 10 min between trains, as previously reported (Quintanilla et al., 2022). For each stimulation frequency, the train's evoked synaptic responses were normalized to the slope of its first synaptic response and plotted as the number of stimuli vs. normalized fEPSP slope (%).

Spatial pattern separation (OPS) task

The spatial pattern separation (OPS) task (based on van Goethem et al., 2018) was performed to evaluate the animals' capacity to discriminate minimal changes in the spatial position of identical objects in a familiar

arena. To reduce the animals' stress from the experimental manipulation, the experimenter manipulated the rats twice per day (2-3 min) for five consecutive days before starting the behavioral evaluations. A circular arena (40 cm high and 83 cm in diameter, gray wall) was placed on a black acrylic platform inside an experimental room with red light. On this platform, a series of reference points' denominated positions (P) were designated as P1 to P5, with 6 cm between the Ps. P1 was aligned at the center of the platform, both left and right, and then P2 to P5 were designated both upward and downward, as depicted in Figure 9a.

The OPS task consisted of two trials (3 min duration each): the learning trial (T1) and the discrimination trial (T2). Before T1 in each evaluation, a habituation phase was carried out, during which the animal was exposed to the empty arena for 5 min. In T1, the animal was introduced to the arena with two identical objects placed in P1 from the left and right of the platform. One hour later, in T2, the animal was re-exposed to the same objects, but one object was displaced to a new position; this then carried on to include all other positions (P2-P5). Object exploration was considered for analysis when the animal explored an object with its nose, with a minimal distance of 2 cm. From the time of exploration for each object, we calculated the discrimination index (DI), a quantitative measurement of the animals' preference for exploring the displaced object over the stationary object, using the following formula:

$$DI = \frac{(displaced\ objects\ exploration\ time - stationary\ object'\ s\ exploration\ time)}{two\ objects\ total\ exploration\ time}$$

To estimate the DI, a minimum exploration time of 7 and 10 s was required for T1 and T2, respectively (van Goethem et al., 2018). Likewise, the performance of each animal for all positions was determined. Therefore, the animals were exposed 5 times to the OPS task with an interval of 2 days and different par objects, which prevented familiarization (van Goethem et al., 2018). The order of evaluation of object positions was random: while one animal began with P1 (without displacement of objects), another animal began with P5 (maximal displacement of one object). After each trial, the platform and the objects were cleaned with ethanol (70%) to eliminate odor residues. The first evaluation of the OPS task was carried out in animals of P30.

Materials

Except for (+)-MK-801 maleate, DCG-IV, L-AP4, and AM 251, which were purchased from Tocris Biosciences (Minneapolis, MN, USA), the drugs and chemicals used in this study were purchased from Sigma Aldrich (St. Louis, MO, USA).

Statistical analysis

Group measures are numerically expressed as mean ± SEM. The violin plots show the median, mean, first, and third quartiles. All statistical comparisons were performed between control values and those obtained from MK-801-treated animals, following the guidelines on experimental design and analysis in pharmacology (Curtis et al., 2018). The normality distribution of data was validated with the Kolmogorov–Smirnov test ($P = 0.05$). No outliers were removed from the data. The comparability among experimental conditions was assessed by two-tailed paired (or unpaired) Student's t-test, Mann-Whitney test, Wilcoxon test, Kruskal-Wallis test, or two-way repeated-measures (RM) analysis of variance (ANOVA), as appropriate. The Holm–Šidák post-hoc or Dunn's post-hoc test was used for multiple comparisons among experimental groups, only when F achieved minimal statistical significance. For all the experiments, data were considered significant if $P < 0.05$.

Results

Criteria for isolating synaptic responses from the medial and lateral perforant paths onto granule cells of the dentate gyrus

The DG granule cells receive glutamatergic inputs via the axons of stellate cells and pyramidal neurons of the lateral and medial EC. These axons, collectively named perforant paths (PP), exhibit unique pharmacological

and synaptic properties depending on whether they originate from the lateral or medial EC (LEC and MEC, respectively). We first isolated and characterized their synaptic responses before exploring whether neonatal treatment with MK-801 alters the LPP and MPP synapses. A stimulation electrode was positioned in the outer one-third section of the molecular layer ([?]200-220 μm above the granule cell layer) or the middle one-third section ([?]100-120 μm above) of the supra-pyramidal blade of the DG (Petersen et al., 2013), and recording pipettes were positioned 200 – 300 μM onto the stimulation electrode to record a fEPSPs from the LPP or MPP, respectively (Figure 1a). Presynaptic terminals of LEC-contacting granule cells selectively express group III metabotropic glutamate receptors (mGluRs), while those of MEC-contacting granule cells express group II mGluRs (Macek et al., 1996; Shigemoto et al., 1997). We used these pharmacological criteria to verify the origin of the evoked responses. Bath perfusion of DCG-IV (5 μM), a group II mGluRs agonist, did not depress the LPP fEPSP (92.9 ± 3.77% of baseline response); however, the subsequent perfusion of L-AP4 (20 μM), a group III mGluRs agonist, abolished the synaptic response (17.18 ± 2.8% of baseline response; $n = 7$ slices / 6 animals, upper traces in Figure 1b). On the other hand, bath perfusion of L-AP4 did not depress the MPP fEPSP (94.8 ± 3.28% of baseline response). However, the synaptic response was abolished during the subsequent application of DCG-IV (20.35 ± 3.2% of baseline response; $n = 7$ slices / 6 animals; lower traces in Figure 1b). The pharmacological activation of mGluRs shows that responses evoked from the LPP and the MPP converging on DG granule cells can be reliably isolated. Therefore, we systematically used these criteria to corroborate the synaptic origins of the evoked responses included in this study.

The transient hypofunction of NMDARs during early postnatal development differentially affects the synaptic strength of the PP – DG synapses.

It is already established that neonatal treatment with MK-801 or related antagonists of NMDA receptors such as phencyclidine alters the glutamatergic transmission of the hippocampus (Kjaerby et al., 2017; Griego et al., 2022; Márquez et al., 2023). Therefore, we explored the effects of MK-801 on the synaptic strength of the LPP and the MPP inputs to DG granule cells. In the control condition, the averaged I-O curve of the LPP fEPSP (0-800 μA; 100 μA steps, at 0.067 Hz) reached a maximal amplitude of 4.16 ± 0.46 mV (black symbols in Figure 1c; $n = 9$ slices / 6 animals); remarkably, neonatal treatment with MK-801 did not alter the maximal amplitude of the LPP fEPSP (maximal amplitude: 3.54 ± 0.34 mV; green symbols in Fig 1c, $n = 10$ slices / 6 animals). Contrary to this observation, the MPP fEPSP reached a maximal amplitude of 7.5 ± 0.68 mV (black symbols in Figure 1d; $n = 8$ slices / 6 animals), and neonatal treatment with MK-801 reduced the maximal MPP fEPSP amplitude to 3.87 ± 0.52 mV ($P < 0.001$ vs. control, two-way RM ANOVA treatment effect: $F_{(1,\ 16)} = 8.31$; red symbols in Figure 1d; $n = 10$ slices / 6 animals). Our findings indicate that neonatal treatment with MK-801 selectively dysregulates the MPP inputs to DG granule cells. While the MPP exhibits a [?]50% reduction in its maximal amplitude, the LPP transmission is not affected by MK-801. Likewise, the pharmacological selectivity of MK-801 suggests a differential composition in the presynaptic and postsynaptic components mediating glutamatergic transmission of the LPP and the MPP onto DG granule cells. In addition, we performed an analysis of the fEPSP kinetics from MPP and LPP synapses; these parameters corroborate the differences in the strength of both synapses (Table 1).

Because the fEPSPs acquired for the I-O curves were preceded by presynaptic fiber volleys (FV), we also analyzed the relationships between stimulus intensity, FV amplitude, and fEPSP amplitude. The left panel in Figure 1e shows the relationship between stimulus intensity (I) and LPP FV amplitude. The right panel depicts the relationship between FV amplitude and LPP fEPSP slope in both experimental conditions (black and green symbols). We found that neonatal treatment with MK-801 did not alter either relationship at the LPP – DG synapse. However, the same analysis at the MPP synapse uncovered a different scenario. The left panel in Figure 1f contrasts the FV response in control vs. MK-801-treated animals (black and red symbols). Compared to the control slices, the MK-801-treated slices exhibited a significant decrease in FV amplitude and faster response saturation [two-way RM ANOVA, interaction effect (treatment x current intensity): $F_{(8,\ 88)} = 2.57$, $P < 0.01$; red symbols; left panel in Figure 1f]. Likewise, the coupling analysis of the FV vs. MPP fEPSP slope shows a dysregulation between FV and MPP fEPSP (slope in control: 0.87 +- 0.24 mV/ms; in MK-801: 0.16 +- 0.04 mV/ms; Mann-Whitney test,$P < 0.01$; right panel in Figure 1f).

These results suggest that neonatal treatment with MK-801 alters the propagation of presynaptic action potentials and the concomitant synaptic response in the MPP but not the LPP synapse.

The transient hypofunction of NMDARs during early postnatal development modifies the paired-pulse ratio at the LPP and the MPP synapses.

Consistent with previous studies (Petersen et al., 2013; Collitti-Klausnitzer et al., 2021), the PPF (60 ms inter-stimulus interval, ISI) differs between the LPP and MPP synapses. We corroborated that the LPP has a prominent PPF (PPF at the LPP – DG = 1.72 +- 0.03;n = 28 slices / 15 animals) compared to the MPP (PPF at the MPP – DG = 1.22 +- 0.03; n = 29 slices / 15 animals; Student's t-test: $t_{(55)}$ = 12.01, $P < 0.001$). Figure 2a shows the PPF distribution of the LPP and the MPP using a violin graph and the responses obtained from 57 independent dorsal hippocampal slices. Figure 2b shows representative examples of facilitation from the LPP and the MPP and their corresponding depression in response to selective activation of group III and II mGluRs, respectively. Because neonatal treatment with MK-801 enhances the PPF at the Mossy Fiber – CA3 pyramidal cell synapse of the rat hippocampus (Segev et al., 2020; Marquez et al., 2023), we performed a similar exploration on the LPP and the MPP using a broader ISI range (40, 60, 100, 200, and 500 ms). The exploration of the LPP PPF revealed increased facilitation in the MK-801 slices compared to control slices (two-way RM ANOVA, treatment effect: $F_{(1, 16)}$ = 5.19, $P< 0.05$; n = 9 slices / 7 animals, for each condition, Figure 2c). The LPP PPF level was statistically increased at 40 and 60 ms (LPP PPF at 40 ms in control: 1.64 +- 0.07; in MK-801: 2.01+- 0.01; $t_{(16)}$ = 2.57, $P < 0.05$; at 60 ms: 1.74 +- 0.06; in MK-801: 1.99 +- 0.06; $t_{(16)}$ = 2.9, $P< 0.01$; at 100 ms: 1.71 +- 0.02; in MK-801: 1.79 +- 0.04; $t_{(16)}$ = 1.5, $P > 0.05$). The temporal change in the PPF is depicted in the representative traces of Figure 2d.

The MPP PPF also showed increased facilitation in the MK-801-treated slices (n = 9 slices / 7 animals) compared to control slices (n = 8 slices / 6 animals; two-way RM ANOVA, treatment effect: $F_{(1, 15)}$ = 4.63, $P < 0.05$; Figure 2e). The facilitation was limited to the ISI of 200 ms (PPF at 60 ms in control: 1.32 +- 0.06; in MK-801: 1.52 +- 0.08; $t_{(15)}$ = 1.854,$P > 0.05$; at 100 ms: 1.3 +- 0.06; in MK-801: 1.51 +- 0.09; $t_{(15)}$ = 1.77, $P < 0.05$; at 200 ms: 1.16 +- 0.05; in MK-801: 1.36 +- 0.04; $t_{(15)}$ = 2.95,$P < 0.01$; representative traces in Figure 2f). The increased PPF observed in the LPP and the MPP synapses suggests a dysregulation in the presynaptic machinery that controls glutamate release on the DG granule cells.

Low-frequency stimulation induces the MPP long-term depression dependent on the cannabinoid receptor type 1.

Thus far, our data show decreased synaptic strength and altered control of glutamate release of the PP terminals synapsing DG granule cells. Previous studies demonstrated that those MK-801-driven changes negatively impact the induction of long-term synaptic plasticity in the hippocampus (Griego et al., 2022; Marquez et al., 2023). Therefore, it is reasonable to assume that neonatal treatment with MK-801 will negatively impact the induction of long-term plasticity at the PP synapses on DG granule cells of the hippocampus.

However, since long-term depression has been scarcely explored in the PP – DG synapses, we first determined a reliable stimulation protocol to induce LTD. Our exploratory experiments show that low-frequency stimulation (LFS, 900 pulses, 1 Hz), a protocol commonly used to induce glutamatergic LTD in the hippocampus (Dudek and Bear, 1992), fails to induce stable synaptic depression in both the LPP – DG and the MPP – DG synapse. In the LPP – DG synapse, LFS did not alter the baseline response (fEPSP at 50 min post-LFS: 108 +- 7.73% of baseline, n = 4 slices / 4 animals; white symbols and upper traces in Figures 1a and 1b). In the MPP – DG synapse, LFS caused transitory synaptic depression, and the fEPSP returned to baseline values within 50 min (fEPSP at 50 min post-LFS: 93.15 +- 5, n = 5 slices / 4 animals; white symbols and upper traces in supplementary Figure 1d and 1e).

Stellar cells and pyramidal neurons of EC layer II discharge volleys in the delta and theta range (0.4 – 10 Hz) to DG granule cells (Gloveli et al., 1997; Deshmukh et al., 2010). Therefore, we explored whether a stimulation paradigm within this physiological range induces LTD. Contrary to our prediction, we found that

900 pulses delivered at 3 Hz triggered synaptic potentiation in the LPP – DG synapse (fEPSP at 50 min post-LFS: 121.2 +- 9.32% of baseline, $n = 3$ slices / 3 animals; black circles and lower traces in supplementary figures 1a and 1b). This form of synaptic potentiation requires additional investigation beyond the scope of the present study.

In sharp contrast, the delivery of 900 pulses at 3 Hz in the MPP – DG synapse induced stable glutamatergic LTD that lasted up to 50 min (fEPSP at 50 min post-LFS: 69.64 +- 6.65% of baseline, $n = 4$ slices / 4 animals; Mann-Whitney test, $P < 0.05$ vs. LFS at 1 Hz; black circles and lower traces in Figures 1d and 1e). Because the delivery of 900 pulses at 3 Hz induced a reliable LTD in the MPP but not in the LPP synapse, subsequent experiments were restricted to the MPP – DG synapse.

Figure 3a-b summarizes the induction of LTD in the MPP – DG synapse and its sensitivity to perfusion DCG-IV (fEPSP at 90 min post-LFS: 69 +- 6.25% of baseline response,$n = 6$ slices / 6 animals; fEPSP in the presence of DGC-IV: 15.66 +- 2.55% of baseline response, Wilcoxon test, $P < 0.05$ vs. baseline response). Moreover, the induction of MPP LTD was accompanied by an increment in the PPF (MPP PPF in control condition: 1.18 +- 0.08; at 90 min post-LFS: 1.54 +- 0.17; Wilcoxon test, $P< 0.05$; black bars in Figure 3f), indicating presynaptic locus for expression of LTD.

According to a previous study, induction of LTD in the MPP synapse requires the delivery of 6,000 pulses at 10 Hz while simultaneously blocking $GABA_A$ receptors (Penasco et al., 2019). Under these experimental conditions, the authors reported that this form of LTD requires activation of the cannabinoid receptor type 1 (CB_1R). Therefore, our next experiment aimed to determine if CB_1R is required for LTD induced with 3 Hz while maintaining active GABAergic transmission. Consistent with Penasco et al., we found that perfusion of the CB_1R antagonist, AM 251 (5 μM), blocks the induction of LTD (MPP fEPSP at 90 min post-LFS: 119.7 ± 10.94% of baseline response, $n = 4$ slices / 4 animals; lower traces and white symbols in Figure 3a-b and white bars in Figure 3e). The subsequent perfusion of the DCG-IV (5 μM) at the end of experiments corroborated the MPP origin of the synaptic responses (fEPSP in the presence of DCG-IV: 15.7 ± 5.22% of baseline; white bar in Figure 3e). Likewise, perfusion of AM 251 prevented the changes in the MPP PPF observed after the induction of LTD (MPP PPF in AM 251 treated slices in control condition: 1.22 ± 0.1; at 90 min post-LFS: 1.2 ± 0.08; Wilcoxon test, $P > 0.05$; white bars in Figure 3f). Together, these results confirm that the MPP – DG synapse exhibits a stable LTD with a presynaptic locus of expression and requires CB_1R activation.

The transient hypofunction of NMDARs during early postnatal development impairs the CB_1R-dependent LTD at the MPP – DG synapse.

If CB_1R activation is a necessary step for the induction of MPP LTD, and previous studies have documented altered CB_1R functionality in several schizophrenia models (Kaminitz et al., 2014; Szűcs et al., 2016; Osborne et al., 2019), it is plausible that MK-801-treated slices could exhibit altered LTD induction. We tested this prediction by applying LFS (900 pulses at 3 Hz) to the MK-801-treated slices. As shown in Figure 3d, LFS failed to induce LTD at the MPP – DG synapse. Moreover, the stimulation protocol induced potentiation of the MPP fEPSP (fEPSP at 90 min post-LFS in MK-801-treated slices: 139.7 ± 23.12% of baseline, $n =$ 6 slices / 6 animals, Kruskal-Wallis test, Dunn's post-hoc test, $P < 0.05$ vs. control; traces and red bars in Figure 3c-d). The synaptic response was sensitive to perfusion of DCG-IV, confirming its presynaptic MPP nature (fEPSP in the presence of DCG-IV: 42.13 ± 8.5% of baseline, Kruskal-Wallis test, Dunn's post-hoc test, $P < 0.05$ vs. control; red bars in Figure 3e). Interestingly, the anomalous synaptic potentiation observed in the MK-801-treated slices did not alter the MPP PPF (PPR in control condition: 1.43 ± 0.07; at 90 min post-LFS: 1.5 ± 0.09; Wilcoxon test, $P> 0.05$; red bars in Figure 3f), suggesting altered functionality of postsynaptic glutamate receptors. The cumulative probability chart in Figure 3g summarizes the magnitude of the MPP LTD observed in control slices (black line), the blockade of LTD in the presence of AM 251 (gray line), and the synaptic response of MK-801-treated slices (red line). These results demonstrate that transient hypofunction of NMDARs during early postnatal development impairs the presynaptic-mediated, CB_1R-dependent LTD and triggers aberrant forms of synaptic plasticity in the MPP – DG synapse.

The transient hypofunction of NMDARs during early postnatal development alters the functional expression of CB_1R in the MPP – DG synapse.

Given CB_1R's critical role in the induction of LTD, we next examined the functional expression of CB_1R in the MPP – DG synapse. We hypothesized that pharmacological activation of CB_1R would fail to induce synaptic depression in the MK-801-treated slices. To test this prediction, we acquired a stable baseline of MPP fEPSPs for 20 min prior to perfusing WIN 55,212-2, a CB_1R agonist (WIN, 5 μM; 15 min). Recording continued up to 90 min, followed by perfusion of DCG-IV. In the control condition, we found that WIN triggers a stable synaptic depression in the MPP – DG synapse, sensitive to DCG-IV (fEPSP 90 min post-WIN: 43.01 ± 6.53% of baseline, $n = 6$ slices / 5 animals; fEPSP in the presence of DCG-IV: 11.23 ± 4.89% of baseline; traces and black bars in Figure 4a-b, e). By contrast, perfusion of WIN in the MK-801-treated slices decreased the magnitude of the synaptic depression of the MPP fEPSP (fEPSP 90 min post-WIN: 74.11 ± 12.16% of baseline, $n = 6$ slices / 6 animals, Student's t-test: $t_{(10)} = 2.25$, $P < 0.05$ vs. control; fEPSP in the presence of DCG-IV: 28.89 ± 4.61% of baseline; traces and red bars in Figure 4a-b, e), suggesting functional dysregulation of presynaptically expressed CB_1R.

Because presynaptic activation of CB_1R requires postsynaptic synthesis and release of 2-AG, we next investigated if neonatal treatment with MK-801 interferes with the postsynaptic synthesis and release of 2-AG. We stimulated the local production of 2-AG by perfusing the cholinesterase inhibitor physostigmine (10 μM) and recording the MPP fEPSPs. After a stable baseline was acquired for 20 min, physostigmine was perfused (10 μM for 15 min). Recording continued up to 90 min and was followed by the perfusion of DCG-IV. In the control condition, physostigmine perfusion induced synaptic depression, sensitive to DCG-IV (fEPSP 90 min post-physostigmine: 52.45 ± 7.06% of baseline, $n = 6$ slices / 6 animals; fEPSP in the presence of DCG-IV: 9.38 ± 1.2% of baseline; traces and black bars in Figure 4c-d, f). Strikingly, in the MK-801-treated slices, physostigmine induced a seemingly diminished synaptic depression, sensitive to DCG-IV (fEPSP 90 min post-physostigmine: 77.65 ± 9.65% of baseline, $n = 5$ slices / 5 animals, Student's t-test: $t_{(9)} = 2.15$; $P > 0.05$ vs. control; fEPSP in the presence of DCG-IV: 30.27 ± 1.97% of baseline; traces and red bars in Figure 4c-d, f). The magnitude of the synaptic depression observed in both WIN and physostigmine in the MK-801-treated slices was similar (Figure 4g), suggesting that 2-AG production in granule cells is not affected by transient hypofunction of NMDARs during early postnatal development. Likewise, the reduced synaptic depression observed in the MK-801 in the presence of physostigmine may be ascribed to dysregulated CB_1R functionality. This possibility requires further exploration.

The inhibition of monoacylglycerol lipase responsible for 2-AG breakdown restores the impaired CB_1R-dependent LTD in MK-801-treated slices.

We reasoned that the impaired LTD may be partially explained by insufficient production or accelerated breakdown of 2-AG during synaptic stimulation. Previous studies have documented increased activity of monoacylglycerol lipase (MAGL), the enzyme responsible for 2-AG degradation, in schizophrenic individuals and experimental models of schizophrenia (Du et al., 2013; Kaya et al., 2019). Therefore, we examined whether increasing 2-AG signaling by inhibiting MAGL activity might restore the electric induction of LTD in the MK-801-treated slices. For these experiments, MK-801-treated slices were perfused with the irreversible MAGL inhibitor, JZL 184 (1 μM, perfused for the last 10 minutes of the baseline response and the first 5 minutes during LFS). Before LFS, the application of JZL 184 did not modify the baseline response. More importantly, JZL 184 reverted the loss of LTD at the MPP – DG synapse of the MK-801-treated slices for up to 90 min (fEPSP 90 min post-LFS: 58.46 ± 11.68 % of baseline, $n = 5$ slices / 5 animals, Student's t-test: $t_{(9)} = 2.94$, $P< 0.01$ vs. MK-801; traces and blue bars in Figure 5a-c). Perfusion of DCG-IV at the end of the recordings corroborated the MPP origin of the synaptic response (fEPSP in the presence of DCG-IV: 27 ± 7.43% of baseline). Likewise, induction of MPP LTD in the MK-801-treated slices was accompanied by increased MP PPF (PPR in control condition: 1.38 ± 1.11; at 90 min post-LFS: 1.77 ± 0.09; paired Student's t-test: $t_{(4)} = 2.97$, $P < 0.05$; blue bars in Figure 5d), which exhibited similar facilitation magnitude to the control slices (see black bars in Figure 3f). The cumulative probability chart in Figure 5e summarizes the magnitude of the MPP LTD observed in the JZL 184-treated slices (blue line) and the lack of LTD in the

MK-801-treated slices (red line). These findings demonstrate that LTD induction in the MPP – DG synapse of animals treated with MK-801 is restored by using MAGL blockade to reduce 2-AG breakdown and thus enhance its signaling. This supports the notion that MAGL blockade has potentially neuroprotective effects (Ren et al., 2020).

Neonatal hypofunction of NMDARs during early postnatal development impairs the induction of long-term potentiation in the LPP – DG synapse.

Granule cells undergo LTP through multiple stimulation patterns that mimic PP activity impinging on the DG. These stimulation protocols are physiologically and behaviorally relevant (Lopez-Rojas et al., 2016); among them, theta-burst stimulation (TBS) has been successfully used to induce stable LTP at the MPP and LPP synapses (Lopez-Rojas et al., 2016; Vyleta and Snyder, 2021). Therefore, we applied TBS to the LPP to test the effects of neonatal MK-801 on LTP induction. A stable baseline of LPP fEPSP slope was recorded for 20 min prior to TBS [3 episodes repeated at 10 s; each episode included 5 pulses delivered at 100 Hz and repeated 10 times at 5 Hz (Larson and Munkácsy, 2015)]. Recording continued for 90 min and was followed by perfusion of L-AP4 (20 μM). In the control condition, TBS triggered a marked post-tetanic potentiation (LPP PTP), followed by long-lasting LPP fEPSP slope potentiation (fEPSP at PTP: 213.4 ± 23.13% of baseline; fEPSP 90 min post-TBS: 144.6 ±13.28% of baseline; fEPSP in presence of L-AP4: 23.18 ± 3.82% of baseline; $n = 7$ slices / 6 animals, traces and black bars in Figure 6a-b). On the other hand, on the MK-801-treated slices, TBS caused a strong PTP but did not induce a sustained increase in the slope of the fEPSP, as illustrated in the green traces and green symbols in Figure 6a-b (fEPSP at PTP: 239.9 ± 18.28% of baseline; fEPSP 90 min post-TBS: 105.5 ± 10.9% of baseline, Mann-Whitney test, $P< 0.05$ vs. control; fEPSP in presence of L-AP4: 28.01 ± 4.33% of baseline; $n = 7$ slices / 7 animals). Interestingly, by adjusting a best-fit single exponential decay function, we found that decay of PTP (tau, ?) is faster in MK-801-treated slices than control slices, suggesting short-term plasticity dysregulation (? in control: 114 +- 23.38 s; ? in MK-801: 47.03 +- 5.88 s, Mann-Whitney test, $P< 0.05$: inset in Figure 6b).

The bar graphs in Figure 6c summarize the mean PTP, potentiation, and sensitivity to L-AP4, while the symbols represent the individual experiments for the control condition and MK-801-treated slices. The heatmaps in Figure 6d contrast the magnitude of the potentiation obtained in each slice, and the cumulative probability graph in Figure 6e shows the overall potentiation for control slices (black symbols) vs. MK-801-treated slices (green symbols). Together, these experiments show that the potentiation of the LPP fEPSP is sensitive to the transient hypofunction of NMDARs during early postnatal development.

Neonatal hypofunction of NMDARs during early postnatal development does not interfere with the expression of LTP in the MPP – DG synapse.

We also explored the synaptic potentiation of the MPP from control and MK-801-treated slices with the same TBS protocol we delivered at the LPP synapse. A stable baseline response of MPP fEPSPs was recorded for 20 min. This was followed by TBS and 90 min of continuous recording and then, finally, perfusion of DCG-IV (5 μM). In the control slices, MPP TBS triggered a PTP and a robust, long-lasting enhancement of the MPP fEPSP slope, sensitive to DCG-IV (fEPSP at PTP: 199.8 ± 11.65% of baseline; fEPSP 90 min post-TBS: 171.4 ± 16% of baseline; fEPSP in presence of DCG-IV: 18.27 ± 2.24% of baseline; $n = 8$ slices / 7 animals; traces and black symbols in Figure 7a-b). Interestingly, MPP TBS delivered on the MK-801-treated slices also triggered PTP, followed by a sustained increase in the slope of the fEPSP not statistically different from the synaptic potentiation observed in the control slices (fEPSP at PTP: 198.9 ± 29.47% of baseline; fEPSP 90 min post-TBS: 135 ± 9.43% of baseline, Mann-Whitney test, $P > 0.05$ vs. control; fEPSP in presence of DCG-IV: 32.46 ± 5.16% of baseline;$n = 7$ slices / 7 animals; traces and red symbols in Figure 7a-b). Likewise, we did not find differences in ? values between the control and MK-801-treated slices (? in control: 65 +- 3 s; ? in MK-801: 83.94 +- 16.34 s, Mann-Whitney test, $P > 0.05$: inset in Figure 7b).

The average post-TBS responses at 90 min for the slices analyzed in the control condition and MK-801-treated slices are depicted in the bar graphs in Figure 7c. The heatmaps in Figure 7d contrast the magnitude of the synaptic potentiation obtained in each slice, and the cumulative probability graph in Figure 7e shows the

potentiation for control slices (black symbols) vs. MK-801-treated slices (red symbols). These results suggest that transient hypofunction of NMDA receptors during early postnatal development does not suppress the MPP – DG synapse's ability to undergo LTP in young rats.

Transient hypofunction of NMDARs during early postnatal development impairs the frequency-dependent synaptic filtering in the LPP – DG synapse.

A specialized feature of the LPP – DG synapse is that it operates as a low-pass filter (Quintanilla et al., 2022). That is, while low frequencies, such as those in the theta range, are efficiently transferred to the DG, the high frequency patterns, i.e., the gamma range, are greatly attenuated upon arrival to the DG. Therefore, in the next experiment, we examined the frequency-dependent filtering property of the LPP – DG synapse by delivering stimulation frequencies relevant to hippocampal cognitive processing, such as the theta (5 Hz), beta (20 Hz), and low gamma (50 Hz) stimulation ranges (Engel and Fries, 2010; Colgin, 2016).

Consistent with Quintanilla et al. (2022), in control slices, a theta train (10 pulses at 5 Hz) induced sustained facilitation all over the evoked synaptic responses (n = 9 slices / 6 animals; traces and black symbols in Figures 8a1 and 8b1). The traces in Figure 8c1 also depict the facilitated response, which contrasts the amplitude of the first response vs. the last response (S1/S10). In contrast, the MK-801-treated slices exhibited greater facilitation in response to 5 Hz stimulation (n = 7 slices / 7 animals). The green symbols of the scatter plot in Figure 8a1 show the increased facilitation of the LPP fEPSPs in MK-801-treated slices compared to control slices (RM two-way ANOVA, treatment effect: $F_{(1,\ 14)} = 7.553$, $P< 0.05$; green traces in Figure 8b1), and the increased facilitation in the amplitude of last response vs. first response is depicted in the green traces in Figure 8c1.

On the other hand, in response to 20 Hz stimulation, control slices exhibited increased facilitation on the first part of the train (second to fifth response), which reverted in the last five responses, generating a Gaussian-type facilitation distribution (n = 8 slices / 6 animals; symbols and black traces in Figure 8a2-c2). Contrary to the ability to attenuate the synaptic responses, the MK-801-treated slices exhibited greater facilitation. i.e., decreased filtering ability. However, this phenomenon, illustrated in Figure 8a2, did not show significant differences compared to control slices (RM two-way ANOVA, treatment effect: $F_{(1,\ 15)} = 3.386$, $P > 0.05$; n = 8 slices / 7 animals for MK-801). The representative traces are depicted in Figures 8b2 and 8c2.

The diminished filtering ability of the LPP – DG synapse in MK-801-treated slices was further revealed by stimulation in the gamma frequency range (50 Hz). Under this experimental paradigm, the control slices exhibited enhanced facilitation in the initial portion of the stimulation train (second to fourth response). The facilitation reverted in the middle section and was strongly attenuated in the final section of the train (n = 8 slices / 6 animals; symbols and black traces in Figure 8a3-c3). Although filtering ability was present in the MK-801-treated slices, there was still an easily identifiable decrease under this condition compared to control slices (RM two-way ANOVA, treatment effect: $F_{(1,\ 14)} = 5.285$, $P < 0.05$, n = 8 slices / 7 animals for MK-801; green symbols in Figure 8a3 and green traces in Figures 8b3 and 8c3). The dysregulation in frequency-dependent filtering of LPP in MK-801-treated slices can also be observed in the scatter plot graphs, which show the change in amplitude between the first response and tenth response for each slice at 5, 20, and 50 Hz train (Figure 8d-f), demonstrating reduced synaptic filtering in MK-801-treated slices. These results show that the synaptic property of low-pass filtering of the LPP – DG synapse is dramatically altered in response to the transient hypofunction of NMDARs during early postnatal development.

Transient hypofunction of NMDA receptors impairs spatial discrimination in rats.

It is hypothesized that after the arrival of cortical information conveying two similar experiences or two events close in time, the DG uses a computational process called pattern separation to orthogonalize (or maximize) the differences in the incoming information onto area CA3 (Yassa and Stark, 2011; Santoro, 2013). This neural mechanism is believed to facilitate the proper storage of similar neuronal information as independent events and prevent the overlapping of new memories. We hypothesized that, if the DG's integrity is compromised due to transient hypofunction of NMDARs, the behavioral activity in which the DG participates will also be compromised. To explore this possibility, we evaluated MK-801-treated animals'

ability to discriminate small changes in the spatial configuration of identical objects maintained in a familiar environment (Santoro, 2013). The discrimination index (DI) of this behavioral test was evaluated by alternating the spatial configuration of identical objects in a familiar environment (see Figure 9a for a schematic representation). A series of spatial positions (P) was used to determine the minimal displacement position of one object vs. another at which the animal perceived the change in spatial position. This cognitive ability increases the demand for spatial pattern separation activity (van Goethem et al., 2018).

In control animals, we corroborated that the DI depends on the magnitude of displacement of one object (Figure 9b), a phenomenon previously reported in adult animals (van Goethem et al., 2018). On the other hand, MK-801-treated animals efficiently differentiated the change in the spatial position of objects when displacement was maximal (DI in P5 from control vs. MK-801: 0.41 +- 0.035 vs. 0.43 +- 0.07; $n = 10$ for the control group and $n = 12$ for MK-801 group), and exhibited comparable DI values in the absence of object displacement (DI in P1 from control vs. MK-801: 0.001 +- 0.021 vs. -0.01 +- 0.011). However, when the magnitude of one object's displacement was gradually reduced from P4 to P2, the MK-801-treated animals' discrimination ability was reduced (DI in P4 from control vs. MK-801: 0.38 +- 0.04 vs. 0.17 +- 0.05; DI in P3 from control vs. MK-801: 0.25 +- 0.03 vs. 0.1 +- 0.04; DI in P2 from control vs. MK-801: 0.07 +- 0.03 vs. 0.001 +- 0.01). These differences in DI values were significant at P3 (two-way RM ANOVA, treatment effect: $F_{(1,\ 20)} = 8.225$, $P < 0.01$; Holm–Šidák post-hoc test, $P < 0.05$). The heatmaps in Figure 9c show the spatial discrimination performance for both experimental conditions. Although MK-801-treated animals efficiently discriminate new object positions when the magnitude of the displacement is maximal (P5), their mnemonic ability for spatial discrimination is reduced when the magnitude of displacement of one object is gradually narrowed, a condition that increases the demand of spatial pattern separation (Figure 9d). Together, these results suggest that impaired spatial discrimination in response to transient blockade of NMDARs may reflect impaired pattern separation associated with psychiatric disorders such as schizophrenia (Faghihi and Moustafa, 2015).

Discussion

This study provides experimental evidence of a series of synaptic alterations of the lateral and the medial perforant paths in response to the transient hypofunction of NMDARs. We documented persistent dysregulation in the glutamate release process from the LPP synapse, blunted induction of LPP LTP, and decreased synaptic filtering capability. In the MPP-DG synapse, the altered glutamate release was accompanied by impaired CB_1R-dependent LTD and weakened LTP. Mechanistically, the impairment of MPP LTD was partly due to decreased functional expression of the CB_1R. More importantly, enhancing the 2-AG signaling pathway via pharmacological inhibition of the MAGL enzyme restored the strength of the MPP LTD. At the behavioral level, we show for the first time that transient hypofunction of NMDARs impairs spatial discrimination, a cognitive task in which DG plays a critical role.

Changes in synaptic strength and presynaptic release at the PP synapses

Functionally, the glutamatergic inputs to the DG convey distinct types of somatosensorial information. The MPP conveys spatial information from the MEC, and the LPP transfers multisensorial information from the LEC (Hunsaker et al., 2007; Fernández-Ruiz et al., 2021). Moreover, the synaptic transfer is sustained by axons with unique electrophysiological properties that determine plasticity capabilities and the pace and strength of neurotransmitter release(Petersen et al., 2013; Collitti-Klausnitzer et al., 2021). Those synaptic features have been robustly demonstrated in this study. Consistent with previous works (Segev et al., 2020; Márquez et al., 2023), our FV and PPF analyses revealed that MK-801 alters the FV amplitude (or presynaptic action potentials) and glutamate release. Dysregulation in the propagation of the FV and the subsequent activation of the molecular machinery underlying glutamate release may explain the reduced strength of the glutamatergic transmission found in the MPP synapse. In line with this possibility, transient hypofunction of NMDARs interferes with the functional expression of presynaptic proteins that control neurotransmitter release in animal models of schizophrenia (Maher and LoTurco, 2012; Saggu et al., 2013) and schizophrenic individuals (Egbujo et al., 2016). Finally, the altered neurotransmitter release process in the MPP compared to the LPP synapse of MK-801-treated animals may suggest a marked dysregulation in transferring spatial

information but not non-spatial information from the PP to the DG, a phenomenon that requires additional investigation.

Changes in the induction and expression of synaptic plasticity

Because glutamatergic LTD has been scarcely explored in the PP – DG synapses, a relevant finding of this study was the establishment of a protocol to induce reliable LTD. The exploratory experiments designed to this end showed that electrical stimulation of MPP, but not LPP, induces a stable LTD in response to 900 pulses delivered at 3Hz, a stimulation frequency that mimics the delta–theta range of volley activity of stellar cells and pyramidal neurons of EC layer II synapsing DG granule cells (Gloveli et al., 1997; Deshmukh et al., 2010). In a previous study, Peñasco et al. demonstrated that MPP LTD can be induced with 6000 pulses at 10 Hz, but this required simultaneous blockade of $GABA_A$ receptors and involved activation of the CB_1R (Peñasco et al., 2019). In the present study, LTD was induced with less electrical stimulation, and GABAergic transmission remained active; the resulting LTD was stable for up to 90 minutes without visible signs of a return to the baseline fEPSP value. The LTD was accompanied by increased PPR, indicating a presynaptic locus for its expression. As in Peñasco et al., the MPP LTD reported in our study requires postsynaptic production of 2-AG.

In slices from MK-801-treated animals, LFS induced synaptic potentiation instead of LTD. The absence of LTD may result from presynaptic dysregulation in CB_1R activity, accelerated breakdown of 2-AG, or altered synthesis of 2-AG at the postsynaptic level. The latter is unlikely, since physostigmine induced a synaptic depression like that observed with activation of CB_1R in the MK-801 condition. These findings indicate that MK-801-treated animals maintain functional postsynaptic production of 2-AG, suggesting a potential dysregulation locus at the presynaptic MPP terminals. In this regard, a critical finding of this study was that the blockade of the MAGL enzyme reverted LTD loss in MK-801-treated animals. MAGL is a presynaptically expressed enzyme that metabolizes 2-AG and is essential in multiple physiological processes, including neuroplasticity, cognitive performance, and behavior (Wang et al., 2018a; Zanfirescu et al., 2021). Our results suggest that transient hypofunction of NMDARs interferes with the expression of the MAGL enzyme, affecting the MPP's ability to express long-term depression of glutamatergic transmission.

We also documented that transient hypofunction of NMDARs hinders the induction and expression of TBS-induced LTP in the LPP synapse and attenuates the magnitude but not the expression of LTP in the MPP synapse. While MPP LTP may be induced in MK-801-treated slices through a series of redundant signaling pathways, including CaMKII and PKA-ERK1/2 (Wu et al., 2006; Welsby et al., 2009), that assure its post-synaptic expression, in the LPP – DG synapse, LTP requires postsynaptic synthesis of 2-AG (Wang et al., 2016), presynaptic activation of CB_1R, and increased neurotransmitter release mediated by the non-canonic CB_1R /FAK/ROCK pathway (Wang et al., 2018b). Although we did not investigate the mechanisms underlying the blunted induction of LPP LTP, decreased functional expression of CB_1R receptors or accelerated degradation of 2-AG may explain the absence of LTP observed in this study.

Changes in the synaptic filtering at the lateral PP

It has been hypothesized that low-pass filtering of synaptic inputs to the DG underlies the encoding information of auditory, olfactory, and visual cues (Scullin and Partridge, 2012; Madar et al., 2019). In this regard, frequency-dependent synaptic filtering of the LPP has been thoroughly characterized in adult mice (Quintanilla et al., 2022). We first confirmed that juvenile rats possess this physiological property; then, we demonstrated that synaptic filtering in the LPP is drastically altered in slices from MK-801-treated animals. Our experimental findings and multiple theoretical models (Chance et al., 1998; Quintanilla et al., 2022) imply that the diminished filtering capacity of the LPP synapse may result from a decreased presynaptic release. The impaired low-pass filtering capability of the LPP could represent the cellular substrate that explains the abnormal processing of sensory information conveyed by the LPP, which is excessively amplified in the DG of schizophrenic individuals (Arnold, 1999; Prasad et al., 2004; Behrendt, 2016) instead of being properly filtered. Although appealing, this idea requires experimental examination.

Behavioral dysregulation

Our spatial discrimination tests suggest that transient hypofunction of NMDARs alters the functional integrity of the DG and thus pattern separation activity, a model of neuronal activity that enables the recognition of independent events despite highly similar information content (Yassa and Stark, 2011). Previous studies have documented reduced volume and alterations in the cellular architecture of the hippocampus and surrounding areas of schizophrenic individuals, with the greatest volume loss in the DG (Nakahara et al., 2019). Volumetric dysregulation also implies changes in the information processing in which DG participates, including pattern separation activity (Faghihi and Moustafa, 2015). In line with this, a recent study has shown deficits in mnemonic discrimination in schizotypal and first-episode psychotic individuals (Kraguljac et al., 2021). We demonstrate for the first time that transient hypofunction of NMDARs impairs spatial discrimination in juvenile male rats. This finding substantiates the idea that impaired mnemonic discrimination is present during the early or prodromal phase of schizophrenia. Consistent with this, recent work showed that children and adolescents at high risk of developing schizophrenia exhibited impaired mnemonic discrimination compared to a control group (İmamoğlu et al., 2023). Given the similar impairments in the mnemonic discrimination task found in our animal model and individuals at high risk for developing schizophrenia, we propose that mnemonic discrimination can be used as a clinical hallmark of the cognitive status of individuals with a high risk of developing schizophrenia. Early screening could allow early therapeutic interventions and modify the course of the illness, as previously suggested (Insel, 2010). At the preclinical level, the animal models that presumably mimic the phenotype schizophrenia should reproduce this impaired mnemonic discrimination in the juvenile stage of animals.

Conclusion

Transient hypofunction of NMDARs with MK-801 alters the synaptic transfer of information from the entorhinal cortex to the dentate gyrus. These changes impact the lateral and medial synapses, dysregulating presynaptic glutamate release, induction of LTD and LTP, and synaptic filtering. Consistent with these alterations, spatial discrimination that depends on pattern separation activity is hindered in the experimental group. These physiological and behavioral dysregulations might account for the reduced cognitive performance observed in schizophrenia. Given its therapeutic potential, future research should consider the modulation of the endocannabinoid system (i.e., CB_1R, 2-AG, or MAGL activity) to restore the synaptic strength and cognitive abilities of individuals at higher risk of developing schizophrenia.

CONFLICT OF INTEREST

The authors declare no competing financial interests.

DECLARATION OF TRANSPARENCY AND SCIENTIFIC RIGOUR

This Declaration acknowledges that this paper adheres to the principles for transparent reporting and scientific rigour of preclinical research as stated in the BJP guidelines for Design and Analysis, and Animal Experimentation, and as recommended by funding agencies, publishers and other organisations engaged with supporting research.

DATA AVAILABILITY STATEMENT

The data that support the findings of this study are available from the corresponding author upon reasonable request.

References

Arnold, O.H. (1999). Schizophrenia – A Disturbance of Signal Interaction between the Entorhinal Cortex and the Dentate Gyrus? The Contribution of Experimental Dibenamine Psychosis to the Pathogenesis of Schizophrenia: A Hypothesis. Neuropsychobiology 40: 21–32.

Behrendt, R.P. (2016). Hallucinatory experience as aberrant event memory formation: Implications for the pathophysiology of schizophrenia. Prog. Neuro-Psychopharmacology Biol. Psychiatry 71: 203–209.

Chance, F.S., Nelson, S.B., and Abbott, L.F. (1998). Synaptic Depression and the Temporal Response Characteristics of V1 Cells. J. Neurosci. 18: 4785–4799.

Colgin, L.L. (2016). Rhythms of the hippocampal network. Nat. Rev. Neurosci. 17: 239–249.

Collitti-Klausnitzer, J., Hagena, H., Dubovyk, V., and Manahan-Vaughan, D. (2021). Preferential frequency-dependent induction of synaptic depression by the lateral perforant path and of synaptic potentiation by the medial perforant path inputs to the dentate gyrus. Hippocampus 31: 957–981.

Curtis, M.J., Alexander, S., Cirino, G., Docherty, J.R., George, C.H., Giembycz, M.A., et al. (2018). Experimental design and analysis and their reporting II: updated and simplified guidance for authors and peer reviewers. Br. J. Pharmacol. 175: 987–993.

Deshmukh, S.S., Yoganarasimha, D., Voicu, H., and Knierim, J.J. (2010). Theta Modulation in the Medial and the Lateral Entorhinal Cortices. J. Neurophysiol. 104: 994–1006.

Du, H., Kwon, I.K., and Kim, J. (2013). Neuregulin-1 Impairs the Long-term Depression of Hippocampal Inhibitory Synapses by Facilitating the Degradation of Endocannabinoid 2-AG. J. Neurosci. 33: 15022–15031.

Dudek, S.M., and Bear, M.F. (1992). Homosynaptic long-term depression in area CA1 of hippocampus and effects of N-methyl-D-aspartate receptor blockade. Proc. Natl. Acad. Sci. 89: 4363–4367.

Egbujo, C.N., Sinclair, D., and Hahn, C.G. (2016). Dysregulations of Synaptic Vesicle Trafficking in Schizophrenia. Curr. Psychiatry Rep. 18: 1–10.

Eichenbaum, H. (2004). Hippocampus: Cognitive Processes and Neural Representations that Underlie Declarative Memory. Neuron 44: 109–120.

Engel, A.K., and Fries, P. (2010). Beta-band oscillations — signalling the status quo? Curr. Opin. Neurobiol. 20: 156–165.

Faghihi, F., and Moustafa, A.A. (2015). A computational model of pattern separation efficiency in the dentate gyrus with implications in schizophrenia. Front. Syst. Neurosci. 9: 132405.

Fernández-Ruiz, A., Oliva, A., Soula, M., Rocha-Almeida, F., Nagy, G.A., Martin-Vazquez, G., et al. (2021). Gamma rhythm communication between entorhinal cortex and dentate gyrus neuronal assemblies. Science (80). 372.

Fontaine, C.J., Gräfe, E.L., Pinar, C., Bonilla-Del Río, I., Grandes, P., and Christie, B.R. (2020). Endocannabinoid receptors contribute significantly to multiple forms of long-term depression in the rat dentate gyrus. Learn. Mem. 27: 380–389.

Forsyth, J.K., and Lewis, D.A. (2017). Mapping the Consequences of Impaired Synaptic Plasticity in Schizophrenia through Development: An Integrative Model for Diverse Clinical Features. Trends Cogn. Sci. 21: 760–778.

Gloveli, T., Schmitz, D., Empson, R.M., and Heinemann, U. (1997). Frequency-dependent information flow from the entorhinal cortex to the hippocampus. J. Neurophysiol. 78: 3444–9.

Goethem, N.P. van, Hagen, B.T.J. van, and Prickaerts, J. (2018). Assessing spatial pattern separation in rodents using the object pattern separation task. Nat. Protoc. 13: 1763–1792.

Griego, E., Hernández-Frausto, M., Márquez, L.A., Lara-Valderrabano, L., López Rubalcava, C., and Galván, E.J. (2022). Activation of D1/D5 receptors ameliorates decreased intrinsic excitability of hippocampal neurons induced by neonatal blockade of N-methyl-d-aspartate receptors. Br. J. Pharmacol. 179: 1695–1715.

Hunsaker, M.R., Mooy, G.G., Swift, J.S., and Kesner, R.P. (2007). Dissociations of the Medial and Lateral Perforant Path Projections Into Dorsal DG, CA3, and CA1 for Spatial and Nonspatial (Visual Object) Information Processing. Behav. Neurosci. 121: 742–750.

İmamoğlu, A., Wahlheim, C.N., Belger, A., and S. Giovanello, K. (2023). Impaired mnemonic discrimination in children and adolescents at risk for schizophrenia. Schizophrenia 9: 1–8.

Insel, T.R. (2010). Rethinking schizophrenia. Nature 468: 187–193.

Jeevakumar, V., Driskill, C., Paine, A., Sobhanian, M., Vakil, H., Morris, B., et al. (2015). Ketamine administration during the second postnatal week induces enduring schizophrenia-like behavioral symptoms and reduces parvalbumin expression in the medial prefrontal cortex of adult mice. Behav. Brain Res. 282: 165–175.

Kaminitz, A., Barzilay, R., Segal, H., Taler, M., Offen, D., Gil-Ad, I., et al. (2014). Dominant negative DISC1 mutant mice display specific social behaviour deficits and aberration in BDNF and cannabinoid receptor expression. World J. Biol. Psychiatry 15: 76–82.

Kaya, M.C., Bulut, M., Kaplan, İ., and Gunes, M. (2019). Levels of endocannabinoid metabolizing enzymes are not related with BDNF levels in patients with schizophrenia: a case-controlled study. Psychiatry Clin. Psychopharmacol. 29: 441–445.

Kjaerby, C., Hovelsø, N., Dalby, N.O., and Sotty, F. (2017). Phencyclidine administration during neurodevelopment alters network activity in prefrontal cortex and hippocampus in adult rats. J. Neurophysiol. 118: 1002–1011.

Kraguljac, N.V., Carle, M., Frölich, M.A., Tran, S., Yassa, M.A., White, D.M., et al. (2021). Mnemonic Discrimination Deficits in First-Episode Psychosis and a Ketamine Model Suggest Dentate Gyrus Pathology Linked to NMDA Receptor Hypofunction. Biol. Psychiatry Cogn. Neurosci. Neuroimaging 6: 1185–1192.

Larson, J., and Munkácsy, E. (2015). Theta-burst LTP. Brain Res. 1621: 38–50.

Li, J.T., Zhao, Y.Y., Wang, H.L., Wang, X.D., Su, Y.A., and Si, T.M. (2015). Long-term effects of neonatal exposure to MK-801 on recognition memory and excitatory-inhibitory balance in rat hippocampus. Neuroscience 308: 134–143.

Lilley, E., Stanford, S.C., Kendall, D.E., Alexander, S.P.H., Cirino, G., Docherty, J.R., et al. (2020). ARRIVE 2.0 and the British Journal of Pharmacology: Updated guidance for 2020. Br. J. Pharmacol. 177: 3611–3616.

Lopez-Rojas, J., Heine, M., and Kreutz, M.R. (2016). Plasticity of intrinsic excitability in mature granule cells of the dentate gyrus. Sci. Rep. 6: 21615.

Lopez-Rojas, J., Solis, C.A. de, Leroy, F., Kandel, E.R., and Siegelbaum, S.A. (2022). A direct lateral entorhinal cortex to hippocampal CA2 circuit conveys social information required for social memory. Neuron 110: 1559-1572.e4.

Macek, T.A., Winder, D.G., Gereau IV, R.W., Ladd, C.O., and Conn, P.J. (1996). Differential involvement of group II and group III mGluRs as autoreceptors at lateral and medial perforant path synapses. J. Neurophysiol. 76: 3798–3806.

Madar, A.D., Ewell, L.A., and Jones, M. V. (2019). Temporal pattern separation in hippocampal neurons through multiplexed neural codes. PLOS Comput. Biol. 15: e1006932.

Maher, B.J., and LoTurco, J.J. (2012). Disrupted-in-Schizophrenia (DISC1) Functions Presynaptically at Glutamatergic Synapses. PLoS One 7: e34053.

Márquez, L.A., Griego, E., López Rubalcava, C., and Galván, E.J. (2023). NMDA receptor activity during postnatal development determines intrinsic excitability and mossy fiber long-term potentiation of CA3 pyramidal cells. Hippocampus 33: 906–921.

Nadel, L., Hupbach, A., Gomez, R., and Newman-Smith, K. (2012). Memory formation, consolidation and transformation. Neurosci. Biobehav. Rev. 36: 1640–1645.

Nakahara, S., Turner, J.A., Calhoun, V.D., Lim, K.O., Mueller, B., Bustillo, J.R., et al. (2019). Dentate gyrus volume deficit in schizophrenia. Psychol. Med. 1–11.

Nakao, K., Jeevakumar, V., Jiang, S.Z., Fujita, Y., Diaz, N.B., Annan, C.A.P., et al. (2019). Schizophrenia-Like Dopamine Release Abnormalities in a Mouse Model of NMDA Receptor Hypofunction. Schizophr. Bull. 45: 138–147.

Nakazawa, K., and Sapkota, K. (2020). The origin of NMDA receptor hypofunction in schizophrenia. Pharmacol. Ther. 205: 107426.

Osborne, A.L., Solowij, N., Babic, I., Lum, J.S., Newell, K.A., Huang, X.F., et al. (2019). Effect of cannabidiol on endocannabinoid, glutamatergic and GABAergic signalling markers in male offspring of a maternal immune activation (poly I:C) model relevant to schizophrenia. Prog. Neuro-Psychopharmacology Biol. Psychiatry 95: 109666.

Peñasco, S., Rico-Barrio, I., Puente, N., Gómez-Urquijo, S.M., Fontaine, C.J., Egaña-Huguet, J., et al. (2019). Endocannabinoid long-term depression revealed at medial perforant path excitatory synapses in the dentate gyrus. Neuropharmacology 153: 32–40.

Petersen, R.P., Moradpour, F., Eadie, B.D., Shin, J.D., Kannangara, T.S., Delaney, K.R., et al. (2013). Electrophysiological identification of medial and lateral perforant path inputs to the dentate gyrus. Neuroscience 252: 154–68.

Prasad, K.M.R., Patel, A.R., Muddasani, S., Sweeney, J., and Keshavan, M.S. (2004). The entorhinal cortex in first-episode psychotic disorders: A structural magnetic resonance imaging study. Am. J. Psychiatry 161: 1612–1619.

Quintanilla, J., Jia, Y., Lauterborn, J.C., Pruess, B.S., Le, A.A., Cox, C.D., et al. (2022). Novel types of frequency filtering in the lateral perforant path projections to dentate gyrus. J. Physiol. 600: 3865–3896.

Ren, S. yu, Wang, Z. zhen, Zhang, Y., and Chen, N. hong (2020). Potential application of endocannabinoid system agents in neuropsychiatric and neurodegenerative diseases—focusing on FAAH/MAGL inhibitors. Acta Pharmacol. Sin. 41: 1263–1271.

Saggu, S., Cannon, T.D., Jentsch, J.D., and Lavin, A. (2013). Potential molecular mechanisms for decreased synaptic glutamate release in dysbindin-1 mutant mice. Schizophr. Res. 146: 254–263.

Santoro, A. (2013). Reassessing pattern separation in the dentate gyrus. Front. Behav. Neurosci. 7: 59930.

Scullin, C.S., and Partridge, L.D. (2012). Modulation by pregnenolone sulfate of filtering properties in the hippocampal trisynaptic circuit. Hippocampus 22: 2184–2198.

Segev, A., Yanagi, M., Scott, D., Southcott, S.A., Lister, J.M., Tan, C., et al. (2020). Reduced GluN1 in mouse dentate gyrus is associated with CA3 hyperactivity and psychosis-like behaviors. Mol. Psychiatry 25: 2832–2843.

Seshadri, S., Klaus, A., Winkowski, D.E., Kanold, P.O., and Plenz, D. (2018). Altered avalanche dynamics in a developmental NMDAR hypofunction model of cognitive impairment. Transl. Psychiatry 2017 81 8: 1–12.

Shigemoto, R., Kinoshita, A., Wada, E., Nomura, S., Ohishi, H., Takada, M., et al. (1997). Differential Presynaptic Localization of Metabotropic Glutamate Receptor Subtypes in the Rat Hippocampus. J. Neurosci. 17: 7503–7522.

Snyder, M.A., and Gao, W.J. (2013). NMDA hypofunction as a convergence point for progression and symptoms of schizophrenia. Front. Cell. Neurosci. 7: 1–12.

Stan, A.D., Ghose, S., Zhao, C., Hulsey, K., Mihalakos, P., Yanagi, M., et al. (2015). Magnetic resonance spectroscopy and tissue protein concentrations together suggest lower glutamate signaling in dentate gyrus in schizophrenia. Mol. Psychiatry 20: 433–439.

Szűcs, E., Dvorácskó, S., Tömböly, C., Büki, A., Kékesi, G., Horváth, G., et al. (2016). Decreased CB receptor binding and cannabinoid signaling in three brain regions of a rat model of schizophrenia. Neurosci. Lett. 633: 87–93.

Tamminga, C.A., Stan, A.D., and Wagner, A.D. (2010). The hippocampal formation in schizophrenia. Am. J. Psychiatry 167: 1178–93.

Vyleta, N.P., and Snyder, J.S. (2021). Prolonged development of long-term potentiation at lateral entorhinal cortex synapses onto adult-born neurons. PLoS One 16: e0253642.

Wang, W., Cox, B.M., Jia, Y., Le, A.A., Cox, C.D., Jung, K.M., et al. (2018a). Treating a novel plasticity defect rescues episodic memory in Fragile X model mice. Mol. Psychiatry 23: 1798–1806.

Wang, W., Jia, Y., Pham, D.T., Palmer, L.C., Jung, K.M., Cox, C.D., et al. (2018b). Atypical Endocannabinoid Signaling Initiates a New Form of Memory-Related Plasticity at a Cortical Input to Hippocampus. Cereb. Cortex 28: 2253–2266.

Wang, W., Trieu, B.H., Palmer, L.C., Jia, Y., Pham, D.T., Jung, K.M., et al. (2016). A Primary Cortical Input to Hippocampus Expresses a Pathway-Specific and Endocannabinoid-Dependent Form of Long-Term Potentiation. ENeuro 3: 10049–10053.

Welsby, P.J., Rowan, M.J., and Anwyl, R. (2009). Intracellular mechanisms underlying the nicotinic enhancement of LTP in the rat dentate gyrus. Eur. J. Neurosci. 29: 65–75.

Wu, J., Rowan, M.J., and Anwyl, R. (2006). Long-term potentiation is mediated by multiple kinase cascades involving CaMKII or either PKA or p42/44 MAPK in the adult rat dentate gyrus in vitro. J. Neurophysiol. 95: 3519–3527.

Yassa, M.A., and Stark, C.E.L. (2011). Pattern separation in the hippocampus. Trends Neurosci. 34: 515–525.

Zanfirescu, A., Ungurianu, A., Mihai, D.P., Radulescu, D., and Nitulescu, G.M. (2021). Targeting monoacylglycerol lipase in pursuit of therapies for neurological and neurodegenerative diseases. Molecules 26: 5668.

Figure legends

FIGURE 1. Neonatal treatment with MK-801 selectively reduces synaptic strength in the MPP – DG synapse. (a) Schematic representation of the EC – DG circuit and placement of stimulation and recording electrodes for extracellular recordings. Stimulation of the lateral perforant path (LPP) and the resulting LPP fEPSP were acquired in the outer one-third section of the molecular layer of the DG (green axons). Medial perforant path or MPP fEPSPs were acquired in the middle one-third of the molecular layer of the DG (red axons). **(b)**Pharmacological sensitivity of the LPP fEPSPs and the MPP fEPSP to different metabotropic glutamate receptors. Upper panel (green traces): LPP fEPSP are sensitive to activation of group III mGluRs with L-AP4 (20 μM) and insensitive to stimulation of group II mGluRs with DCG-IV (5 μM). Lower panel (red traces): MPP fEPSP are insensitive to activation of group III mGluRs. The opposite occurs in the presence of group II mGluRs agonists. The pharmacological sensitivity of the fEPSPs to the different mGluRs was rigorously used as an inclusion criterion for all the experiments included in this study. **(c)** Input-output graphs of the LPP fEPSPs and **(d)** the MPP fEPSPs in response to increasing current pulses (100 μA steps at 0.067 Hz). Neonatal treatment with MK-801 did not alter the magnitude of the LPP fEPSP (upper trace and green symbols in panel c) but reduced the magnitude of the MPP fEPSP (upper trace and red symbols in panel d), $^{**}P < 0.01$.**(e)** Left panel: input-output curve of the LPP fiber volleys (FV) in response to increasing current pulses; right panel: coupling analysis of the FV vs. LPP fEPSP slope, showing no difference in synaptic strength. **(f)** Left panel: input-output curve of the MPP FV in response to increasing current pulses, showing decreased presynaptic excitability in the MK-801 group; right panel: coupling analysis of FV vs. MPP fEPSP slope. * $P < 0.05$ and ** $P < 0.01$. For LPP: $n = 9$ slices / 6 animals for the control group and $n = 10$ slices / 6 animals for the MK-801 group. For MPP: 8 slices / 6 animals for the control group and $n = 10$ slices / 6 animals for the MK-801 group.

FIGURE 2. Neonatal treatment with MK-801 reduces presynaptic neurotransmitter release at the LPP and the MPP. (a) Violin plots contrasting the paired-pulse facilitation values (PPF; ISI 60 ms) of the LPP (n = 28 slices / 15 animals; green symbols) and the MPP (n = 29 slices / 15 animals; red symbols) synapses in the control condition. LPP PPF was greater than MPP PPF, $^{***}P < 0.001$.**(b)** Representative traces showing the pharmacological sensitivity of the LPP and the MPP synapses. LPP PPF decreased in the presence of L-AP4 (20 μM, upper traces), whereas the MPP PPF was abolished by perfusion of DCG-IV (5 μM; lower traces). **(c)** Time course of the LPP PPF exploring different ISI (40, 60, 100, 200, and 500 ms). Neonatal treatment with MK-801 increased the LPP PPF. $^{*}P< 0.05$. For LPP PPF: $n = 8$ slices / 6 animals for control and $n = 9$ slices / 7 animals for MK-801. **(d)**Representative PPF of the LPP synapses contrasting the values of control and MK-801-treated slices. **(e)** Time course and **(f)**representative traces for MPP PPF in control (red symbols and traces) and MK-801-treated (black symbols and traces) slices. MPP PPF: n= 9 slices / 7 animals for each condition. $^{*}P < 0.05$.

FIGURE 3. Neonatal treatment with MK-801 impairs the induction of CB_1R-dependent LTD at the MPP – DG synapse. (a) Representative traces of control (upper traces) and the CB_1R antagonist, AM251 treatment (5 μM, lower traces) in baseline, post-LFS, and the presence of DCG-IV (5 μM). **(b)** Time course graph of fEPSP slope in response to LFS (900 pulses at 3 Hz) in the MPP. In the control condition (black symbols), LFS induces LTD. Perfusion of AM 251 (5 μM, white symbols) LFS prevented the induction of LTD. **(c)** Representative traces of the control (upper black traces) and MK-801-treated group (lower red traces) in baseline, post-LFS, and the presence of DCG-IV (5 μM). **(d)** Time course graph of LTD. In the MK-801-treated group, LFS failed to induce LTD; an abnormal potentiation (red symbols) was observed that was sensitive to DCG-IV (5 μM). **(e)** Bar graph summarizing the magnitude of normalized fEPSP slopes at 90 min after LFS and in the presence of DCG-IV in the control (symbols and black bars), AM-251 (symbols and white bars), and MK-801 (symbols and red bars) groups. $^{*}P< 0.05$. Each symbol within the bars represents one independent experiment; bars represent the media ± SEM. **(f)** Bar graph showing the changes in PPR before and after LFS. The control group exhibited increased PPR after LFS, suggesting a reduction in presynaptic release at the MPP. $^{*}P < 0.05$; n = 6 slices / 6 animals for control and MK-801; n = 4 slices / 4 animals for AM 251.**(g)** Cumulative probability distribution chart of normalized fEPSPs post-LFS in the control (black line), AM-251 (gray line), and MK-801 (red line) groups. The individual values for this analysis (bins configured at 0.8 value) correspond to 10 to 90 minutes of the time course in panels **b** and **c** .

FIGURE 4. Neonatal treatment with MK-801 reduces the functional expression of CB_1R but not the synthesis of 2-AG at the MPP – DG synapse. (a) Representative traces of control and MK-801 fEPSPs during baseline (1), 90 min post-WIN 55,212-2 (2), and DCG-IV (3). **(b)** Time course graph of normalized fEPSP slope in response to the perfusion of the CB_1R agonist, WIN 55,212-2 (5 μM for 15 min), in control and MK-801-treated groups (black and red symbols, respectively). **(c)** Representative traces and**(d)** time course graph of normalized fEPSPs in the presence of the cholinesterase inhibitor physostigmine (10 μM for 15 min) in control and MK-801-treated groups (black and red symbols, respectively). Slices of the MK-801-treated group exhibited synaptic depression in response to physostigmine perfusion. **(e)** Bar graph contrasting the synaptic depression elicited with WIN 55,212-2 in control vs. MK-801-treated groups. $^{*}P < 0.05$, n = 6 slices / 5 animals for control and n = 6 slices / 6 animals for MK-801. **(f)** Bar graph contrasting the magnitude of synaptic depression in response to physostigmine. The MK-801-treated group (red bar) exhibited reduced synaptic depression; however, this difference lacked statistical significance compared to the control group (black bar). n = 6 slices / 6 animals for control and n = 5 slices/ 5 animals for MK-801. **(g)** Bar graph contrasting the magnitude of synaptic depression in the MK-801-treated groups in response to WIN 55,212-2 or physostigmine. The synaptic depression induced by physostigmine is similar to the magnitude of depression induced by activation of CB_1R with WIN, suggesting that 2-AG synthesis is not affected by neonatal treatment with MK-801.

FIGURE 5. Pharmacological inhibition of monoacylglycerol lipase (MAGL) enzyme restores the impaired CB_1R-dependent LTD at the MPP – DG synapse. (a) Representative fEPSP traces from MK-801-treated slices (red traces) or those preincubated with JZL 184 (blue traces) in the conditions

indicated by the numbers. **(b)**Time course graph of normalized fEPSPs from MK-801-treated slices in the presence of the irreversible inhibitor of monoacylglycerol lipase (MAGL JZL 184, 1 μM; blue symbols). LFS induced stable LTD in the presence of JZL 184 MK-801-treated slices. **(c)** Bar graph. Perfusion of JZL 184 rescues LTD at the MPP – DG synapse. *P < 0.05; n = 6 slices / 6 animals for MK-801-treated group and n = 5 slices / 5 animals for MK-801 + JZL 184 group. **(d)** Bar graphs showing restored LTD is accompanied by increased PPR. * P < 0.05. **(e)**Cumulative probability distribution plot of the fEPSP slope values after LFS (red line) or LFS + JZL (blue line) in MK-801-treated slices. The individual values for this analysis (bins configured at 0.8 value) correspond to 10 to 90 minutes of the time course in panel b.

FIGURE 6. Neonatal treatment with MK-801 impairs the TBS-induced LTP at the LPP – DG synapse. (a) Representative traces of fEPSP from control (black traces) and MK-801 (green traces) in the conditions indicated by the numbers. **(b)** Time course of normalized fEPSP slope from control and MK-801 in response to TBS. Arrowhead indicates the delivery of the TBS train (10 bursts at 5 Hz; each burst consisted of 5 pulses at 100 Hz). Inset bar graph comparing the post-tetanic potentiation decay calculated by adjusting a best-fit single exponential decay function. The PTP dropped faster in the MK-801-treated group. $*P < 0.05$. **(c)** Bar graph contrasting the magnitude of PTP, LTP, and the effect of L-AP4 (20 μM) on the LPP synapse. *P < 0.05; n = 7 slices / 6 animals for control and n = 7 slices / 7 animals for MK-801. **(d)** Heatmaps showing the magnitude of LTP in each slice from both experimental groups.**(e)** Cumulative probability distribution plot of the fEPSP slope values. The individual values for this analysis (bins configured at 0.8 value) correspond to 10 to 90 minutes of the time course in panel b.

FIGURE 7. Neonatal treatment with MK-801 does not interfere with the induction of TBS-induced LTP at the MPP – DG synapse. (a) Representative traces of fEPSP from control (black traces) and MK-801 (red traces) in the conditions indicated by the numbers. **(b)**Time course of normalized fEPSP slope in response to TBS. Inset bar graph comparing the post-tetanic potentiation decay calculated by adjusting a best-fit single exponential decay function. No difference was found in either group. **(c)** Bar graph contrasting the magnitude of PTP, LTP, and the effect of DCG-IV (5 μM). n = 8 slices / 7 animals for control and n = 7 slices / 7 animals for MK-801.**(d)** Heatmap showing the magnitude of LTP in each slice from both experimental groups. **(e)** Cumulative probability distribution plot of the fEPSP slope values.

FIGURE 8. Neonatal treatment with MK-801 impairs frequency-dependent synaptic filtering at the LPP. (a1-a3, left panels) Scatter plot showing the evoked fEPSPs slope from control (black symbols) and MK-801-treated (green symbols) groups in response to 5, 20, and 50 Hz trains. In control slices, 5 Hz induced synaptic facilitation throughout the stimulation train, 20 Hz caused a mild synaptic depression at the end of the train, and 50 Hz induced massive attenuation of the synaptic response (horizontal dashed lines represent facilitation value vs. S1). In the MK-801-treated slices, frequency-dependent filtering was impaired at 5 Hz and 50 Hz since synaptic facilitation was increased. *P < 0.05. Train at 5 Hz: n = 9 slices/animals for control and n = 7 slices / 7 animals for MK-801. Train at 20 Hz and 50 Hz: n = 8 slices / 6 animals for control and n = 8 slices / 7 animals for MK-801. **(b1-b3)** Representative traces in response to trains at 5 Hz, 20 Hz, and 50 Hz. **(c1-c3)**Over-imposed traces showing the first synaptic response (S1) vs. the tenth response (S10) in the three frequencies examined. **(d-f)**Bar graphs contrasting the magnitude of the fEPSP amplitude (measured in mV) from S1 and S10 in both experimental conditions at the three frequencies tested.

FIGURE 9. Neonatal treatment with MK-801 impairs spatial discrimination in male rats. (a) Schematic representation of the object spatial pattern separation (OPS) task. The task comprised a learning trial (T1) and a discrimination trial (T2). It was performed in a circular arena with two equidistant identical objects (40 cm) placed in five positions (P), with 6 cm between positions. These positions were designated both left and right from the center of the arena. In T1, the animals were exposed to two objects placed in P1. In T2, both objects were placed in P1 (null displacement), or one was placed in P2, P3, P4, or P5 (maximal displacement). The discrimination index (DI) was indicative of performance in this task. All animals were evaluated in all P values with intervals of two days. Objects in green or gray prism form represent identical par objects. **(b)** Bar graph summarizing the DI values obtained from control (black

bars) and MK-801-treated (blue bars) animals during the OPS task. MK-801-treated animals could not distinguish the displacement of one object to P3, indicating impaired spatial discrimination. *P $<$ 0.05, n = 10 for control and n = 12 for MK-801. **(c)** Heatmap showing all DI values for each animal from both experimental conditions. While the color scale in the P5 columns is similar in control and MK-801-treated animals, the color pattern in the P3 columns differs between experimental conditions, indicating reduced DI values in MK-801-treated animals. **(d)**Line chart summarizing DI performance from control (black line) and MK-801 (blue line) in function of the magnitude of displacement of one object in T2. In control animals, when the magnitude of displacement of one object is decreased, the cognitive demand of pattern separation is theoretically increased, which supports the spatial discrimination of the position of objects. However, when the magnitude of displacement of one object is maximal (24 cm), MK-801-treated animals exhibit similar behavioral performance to control animals. When the cognitive demand of pattern separation increases, the MK-801-treated animals exhibit impaired performance in spatial discrimination.

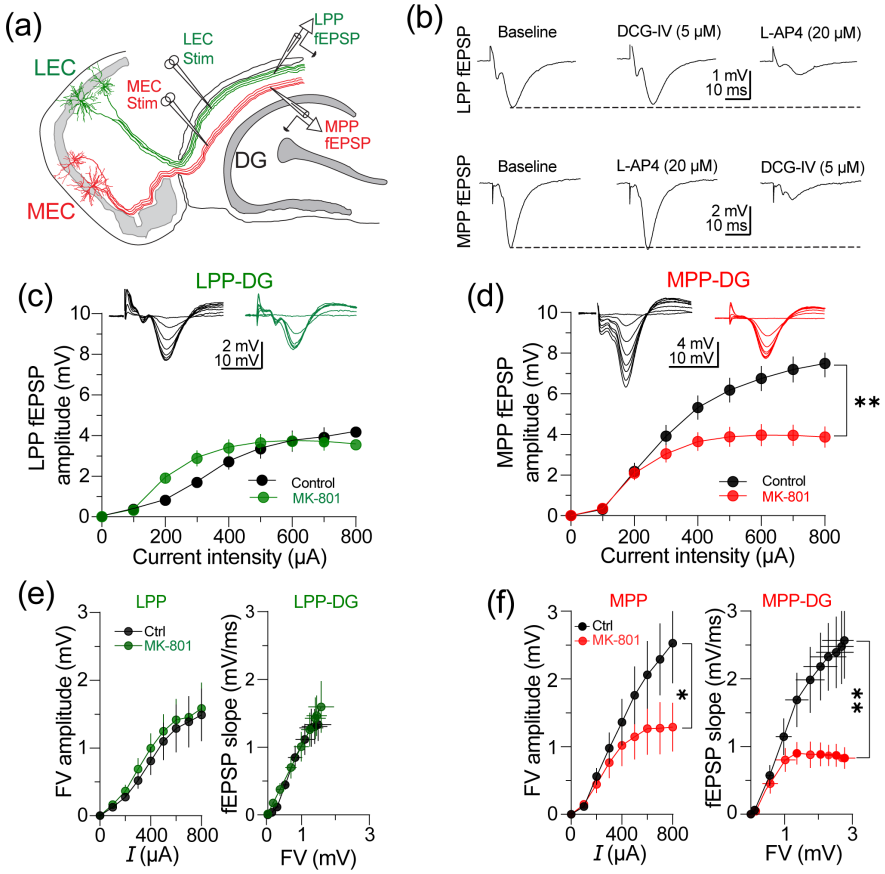

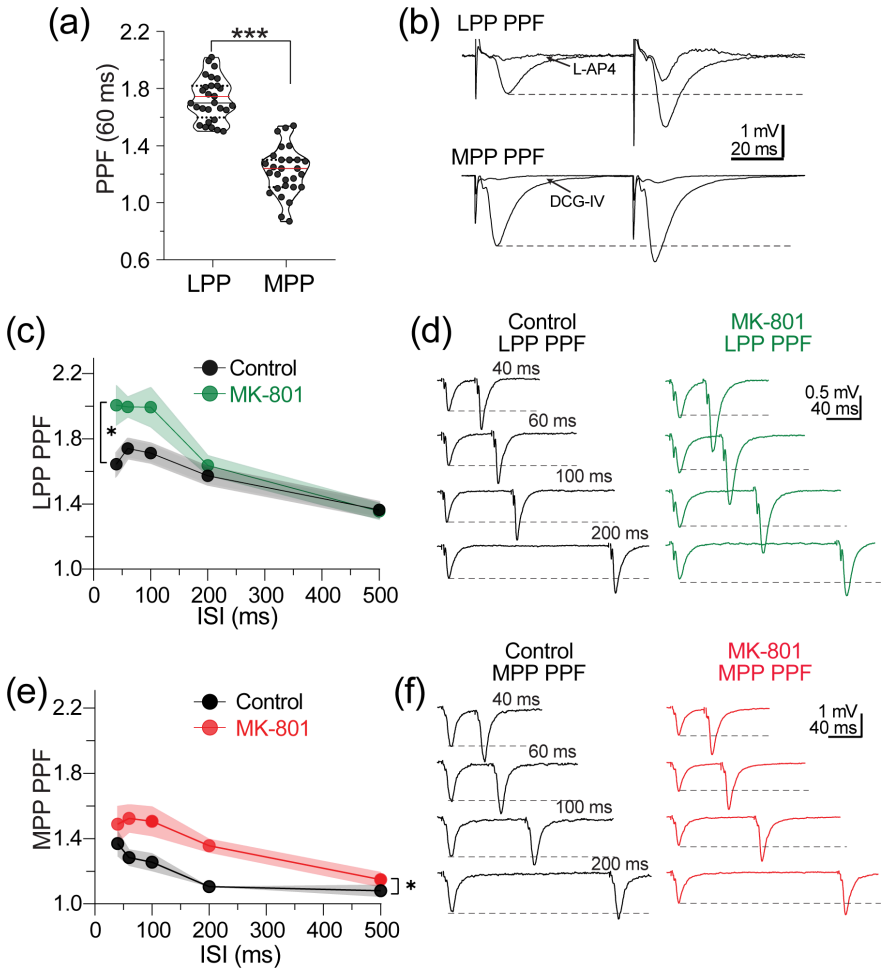

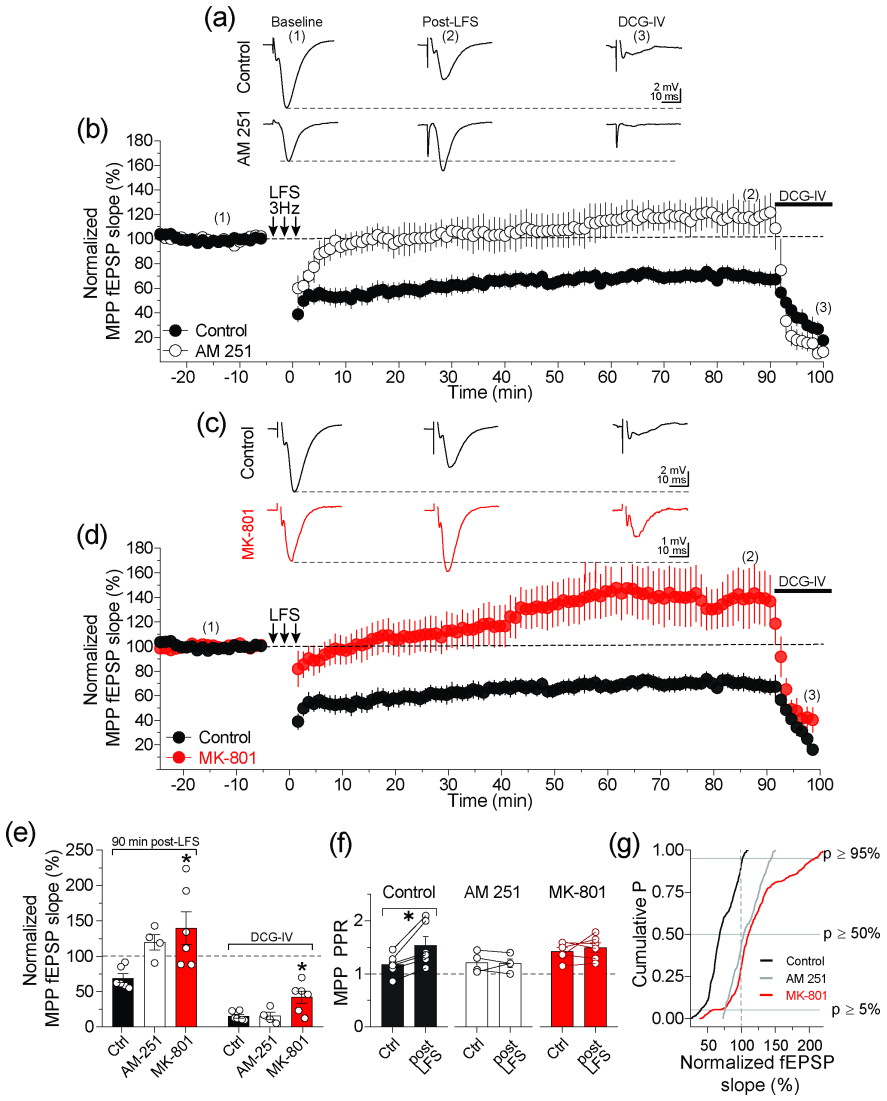

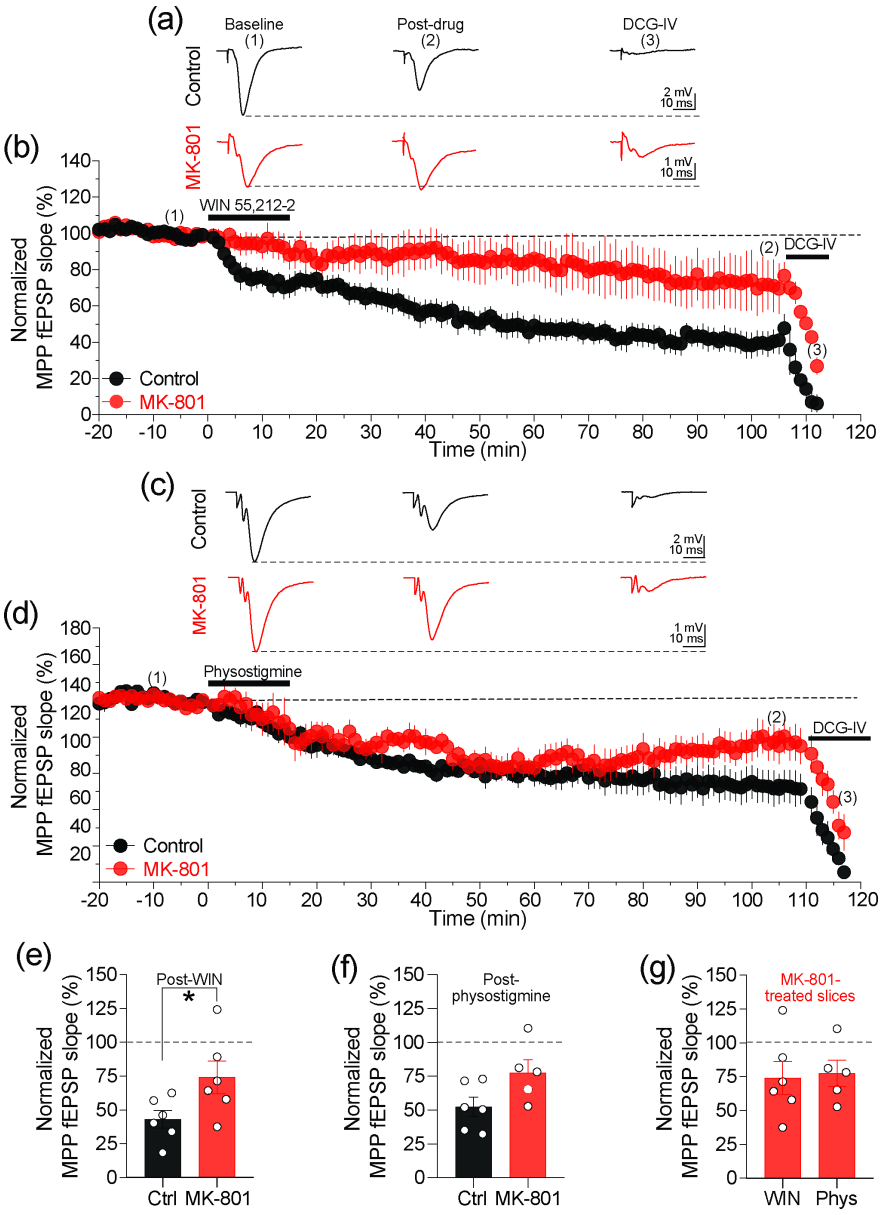

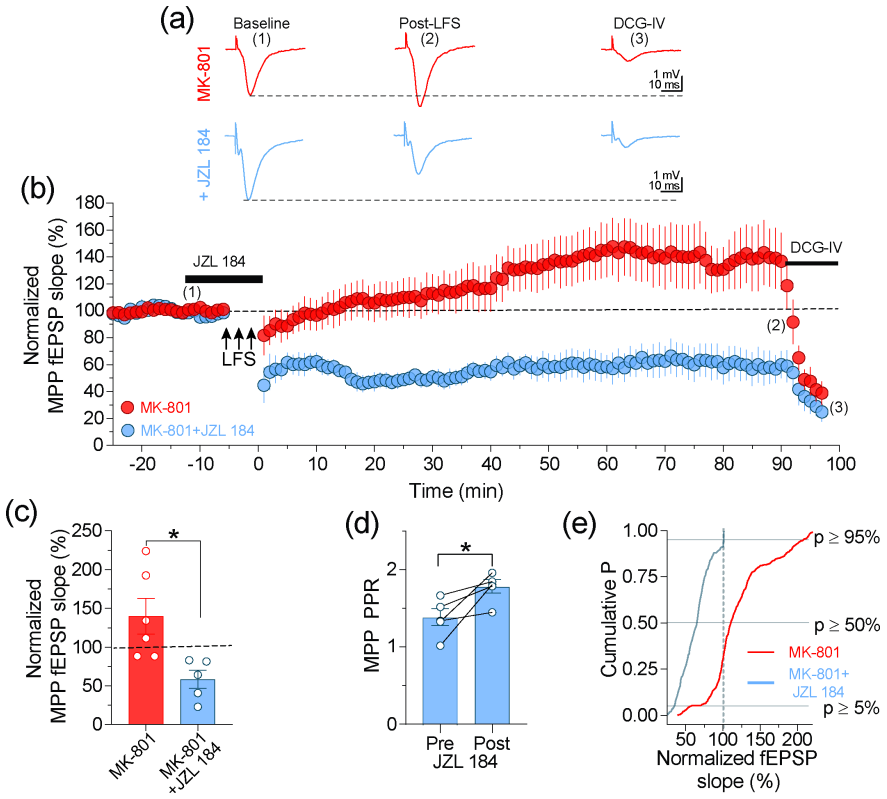

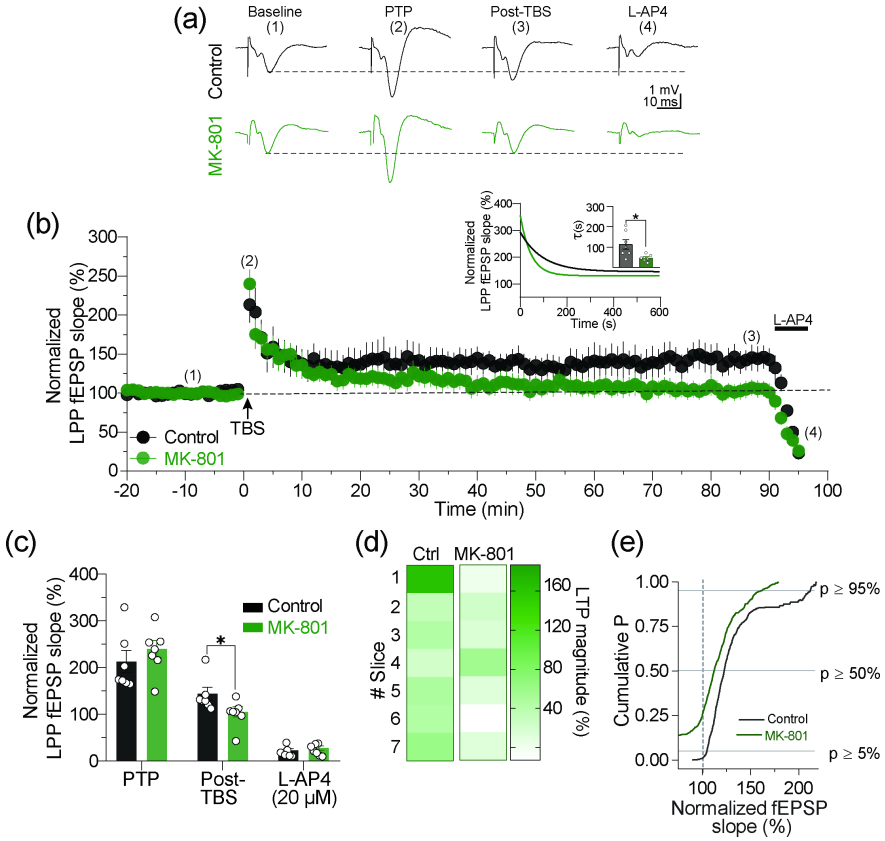

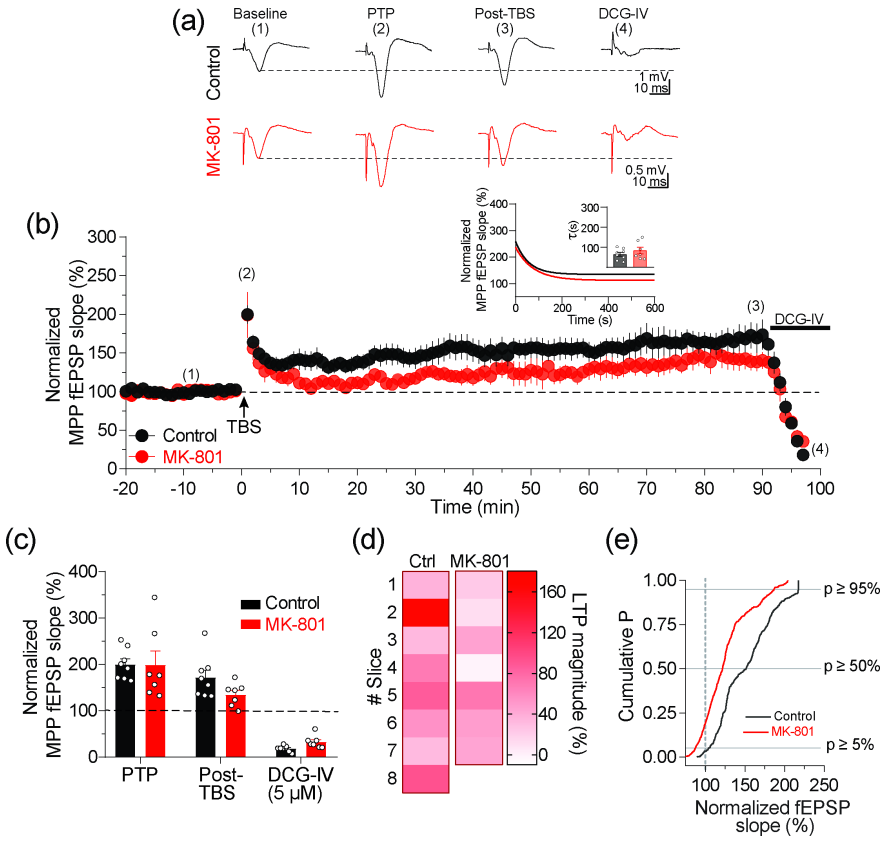

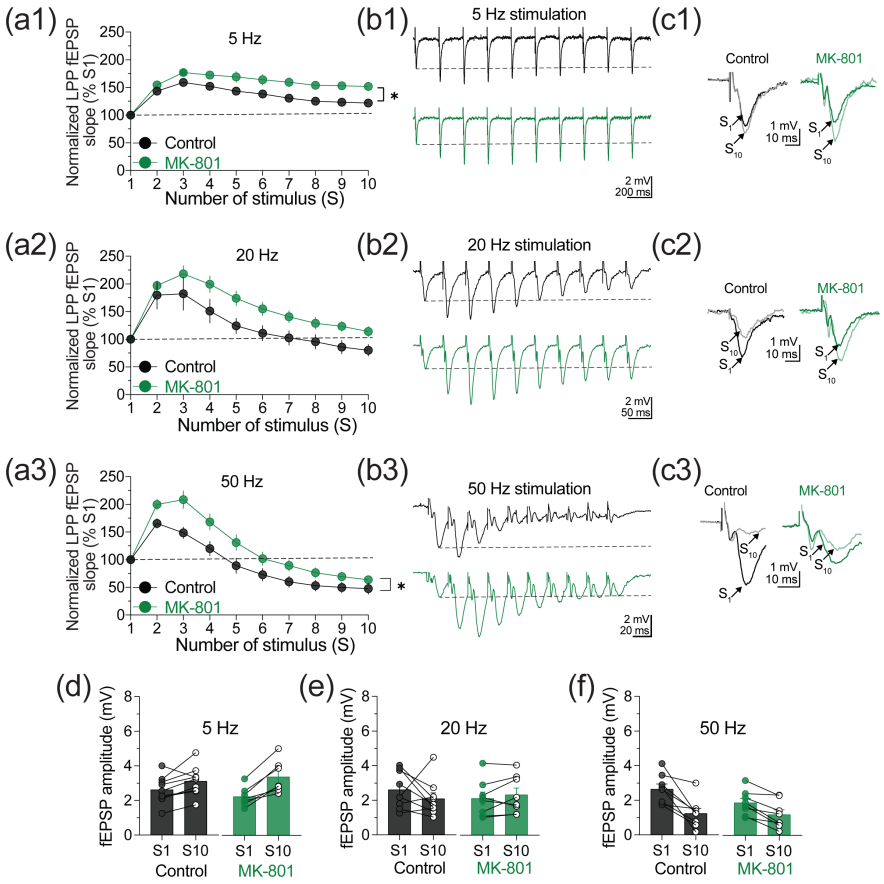

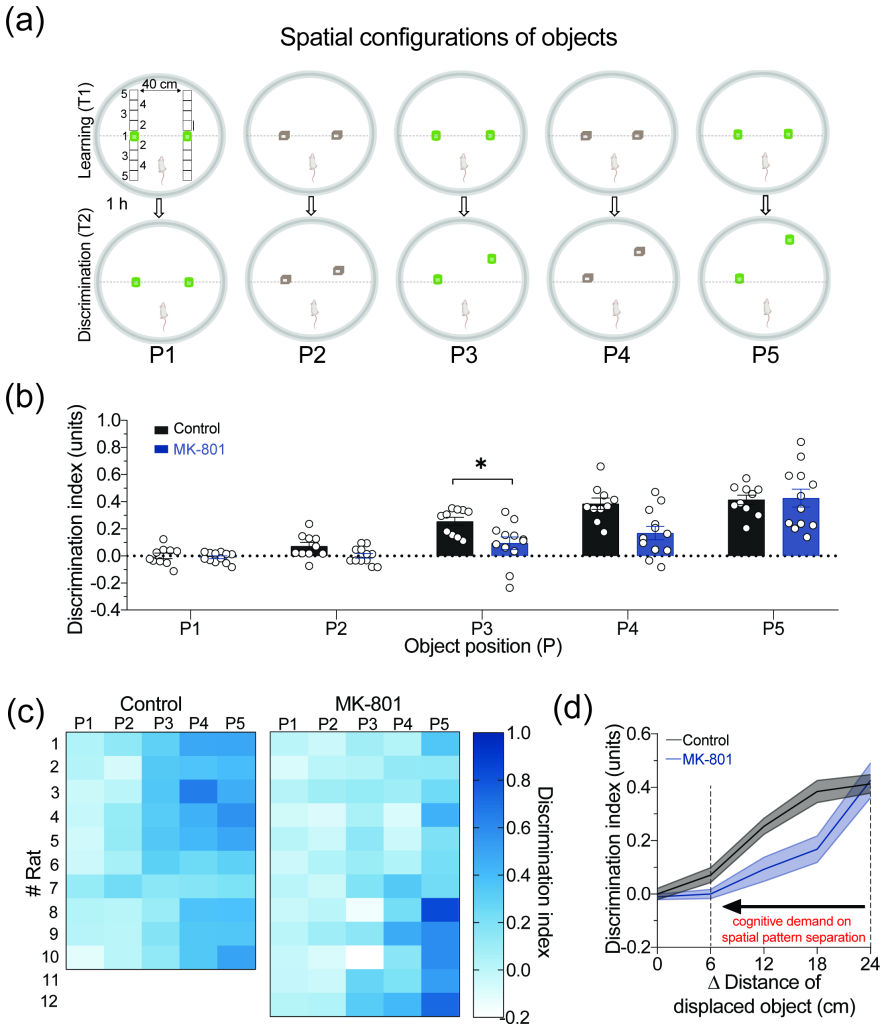

Hosted file

`Sept 04 Table 1.docx` available at https://authorea.com/users/659540/articles/663448-neonatal-hypofunction-of-nmda-receptors-alters-perforant-path-synaptic-plasticity-filtering-and-impairs-dentate-gyrus-mediated-spatial-discrimination